35260

PL-15-FMIR64-1107

FINAL REPORT

FOR

STUDY PROGRAM TO OBTAIN THE INFRARED ABSORPTION SPECTRA OF POWDERED ROCKS

Prepared under

NASA Contract #NASw-964

Prepared for

National Aeronautics and Space Administration
Lunar and Planetary Programs
Washington, D. C.

Prepared by

Philips Laboratories
A Division of North American Philips Company, Inc.
Briarcliff Manor, New York

December 1964

PL-15-FMIR64-1107 TECHNICAL REPORT # 174

FINAL REPORT

FOR

STUDY PROGRAM TO OBTAIN THE INFRARED ABSORPTION SPECTRA OF POWDERED ROCKS

Prepared under

NASA Contract #NASw-964

Prepared for

National Aeronautics and Space Administration
Lunar and Planetary Programs
Washington, D. C.

Prepared by

Philips Laboratories
A Division of North American Philips Company, Inc.
Briarcliff Manor, New York

December 1964

PHILIPS LABORATORIES

PL-15-FMIR64-1107

A B S T R A C T

1628)

This document is the final report for a study program to determine the feasibility of using the technique of Frustrated Multiple Internal Reflection (FMIR) Spectroscopy for obtaining the infrared absorption spectra of powdered rocks. The theory of the FMIR technique is discussed, and the instrumentation of the system used in this study is described. The FMIR infrared absorption spectra of silicate powders (of diameters 0 to 43 μ, 150 μ and 300 μ) were of high spectral quality, and no loss of energy due to light scattering was observed. Experimental results indicate that FMIR Spectroscopy is a feasible method for obtaining high quality infrared absorption spectra of powders and rough solids in their natural state.

Author

TABLE OF CONTENTS

L I S T O F I L L U S T R A T I O N

Page

L I S T O F T A B L E S

1. INTRODUCTION

This document is a final report for a four-month study program conducted by Philips Laboratories, A Division of North American Philips Company, Inc. The purpose of the research study was to determine the feasibility of using the technique of Frustrated Multiple Internal Reflection (FMIR) Spectroscopy to obtain the infrared absorption spectra of powdered rocks.

2. OBJECTIVES

FMIR spectroscopy has made it possible to analyze chemical compounds which are not or cannot be put into a form suitable for investigation by conventional infrared absorption spectroscopy. The technique appears to be a valuable analytical tool for the study of powders.

The objectives of this study program were:

a) Fabrication of an FMIR system (2 to 15 micron wavelength range), including the investigation of several probe (cell) materials.

b) Purchase of quartz powder in several particle sizes.

c) Obtaining FMIR absorption spectra of these powders.

d) Determination of the degree of scattering in the non-absorbing region of these powders.

e) Comparison of spectra of particles in the 10 to 50 micron diameter range.

f) Obtaining FMIR absorption spectra of rough solids such as frosted glass or sand blasted quartz.

3. SUMMARY

3.1 FMIR System

3.1.1 Theory

1. FMIR Principles. Total internal reflection spectroscopy has found numerous applications since the technique was first proposed (Refs. 1, 2, 3, 4). In many applications, distinct advantages are found over conventional absorption techniques. For example, in measuring the absorption spectra of liquids, troublesome interference patterns found in thin liquid cells are eliminated. The strength of the molecular resonance absorption can be adjusted by changing the angle of incidence of the light beam or the volume of sample under investigation.

In Frustrated Multiple Internal Reflection, the surface is sampled many times, and weak absorptions are thus amplified. The advantages thus gained over a single reflection approach are that the spectra of thin films, even monolayer films, can be measured; measurements on bulk materials can be made far from the critical angle; and the resulting spectra more closely resemble those obtained by transmission spectroscopy.

Briefly, the principles of FMIR are the following. With reference to the coordinate system shown in Figure 1, light propagating in the denser medium towards an interface where there is a change in refractive index will be totally reflected when the angle of incidence exceeds the critical angle given by

$$\theta_c = \sin^{-1} n_{21}$$

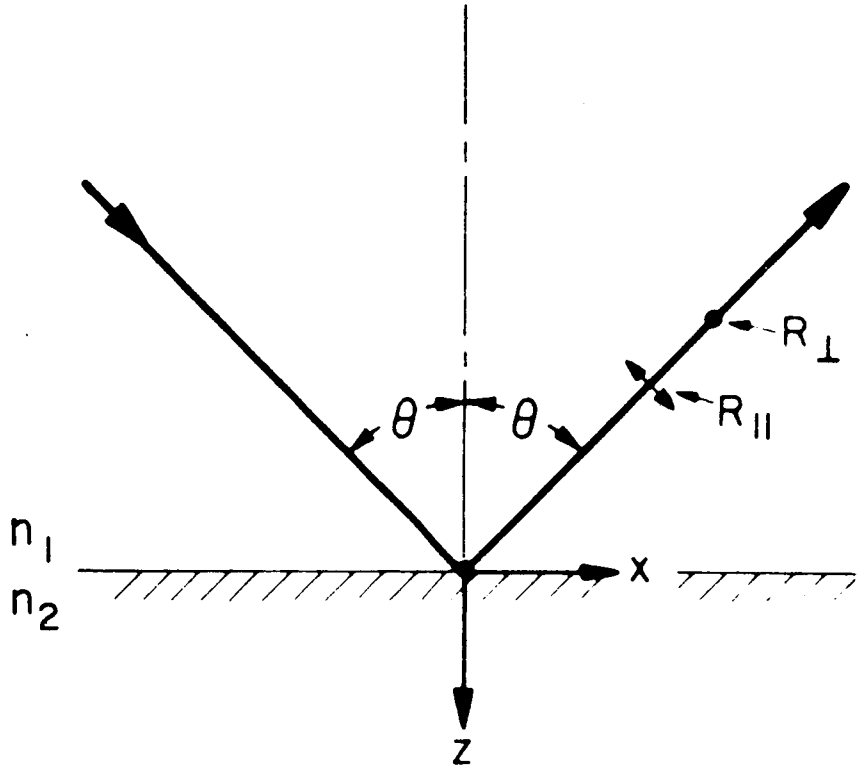

Figure 1: Reference Coordinate System for Light Ray Incident on an Interface Between Two Media (1, 2) Where There is a Change in Refractive Index.

where $n_{21} = n_2 n_1$. As a result of the superposition of the incoming and reflected waves, a standing wave normal to the reflecting interface is established, as shown in Figure 2. In the denser medium, the electric field amplitude varies sinusoidally with distance from the surface. In the rarer medium, however, a nonpropagating wave is found where the electric field amplitude decays exponentially with distance from the surface. The depth of pentration in the rarer medium is defined as the distance required for the electric field amplitude to decay to one-half of its value at the surface and is given by

$$Z_{\frac{1}{2}} = \frac{0.693\lambda_1}{2\pi\,(\sin^2\theta - n_{21}{}^2)^{\frac{1}{2}}}$$

This penetration depth is plotted vs angle of incidence and is shown in Figure 3 for two cases, namely $n_{21} = 0.285$ and $n_{21} = 0.457$. It should be noted that the penetration depth is of the order of one-tenth of the wavelength in the denser medium near grazing incidence but reaches large values near the critical angle. It has been shown in numerous experiments that it is possible to couple or absorb energy from this penetrating electromagnetic field; thus, the reflectance becomes less than total, and the reflection is thus frustrated.

For most of the measurements on surface phenomena, the thickness of the films involved is considerably less than a penetration depth, hence variation of the magnitude of penetration depth with θ does not cause displacement or distortion of the absorption band.

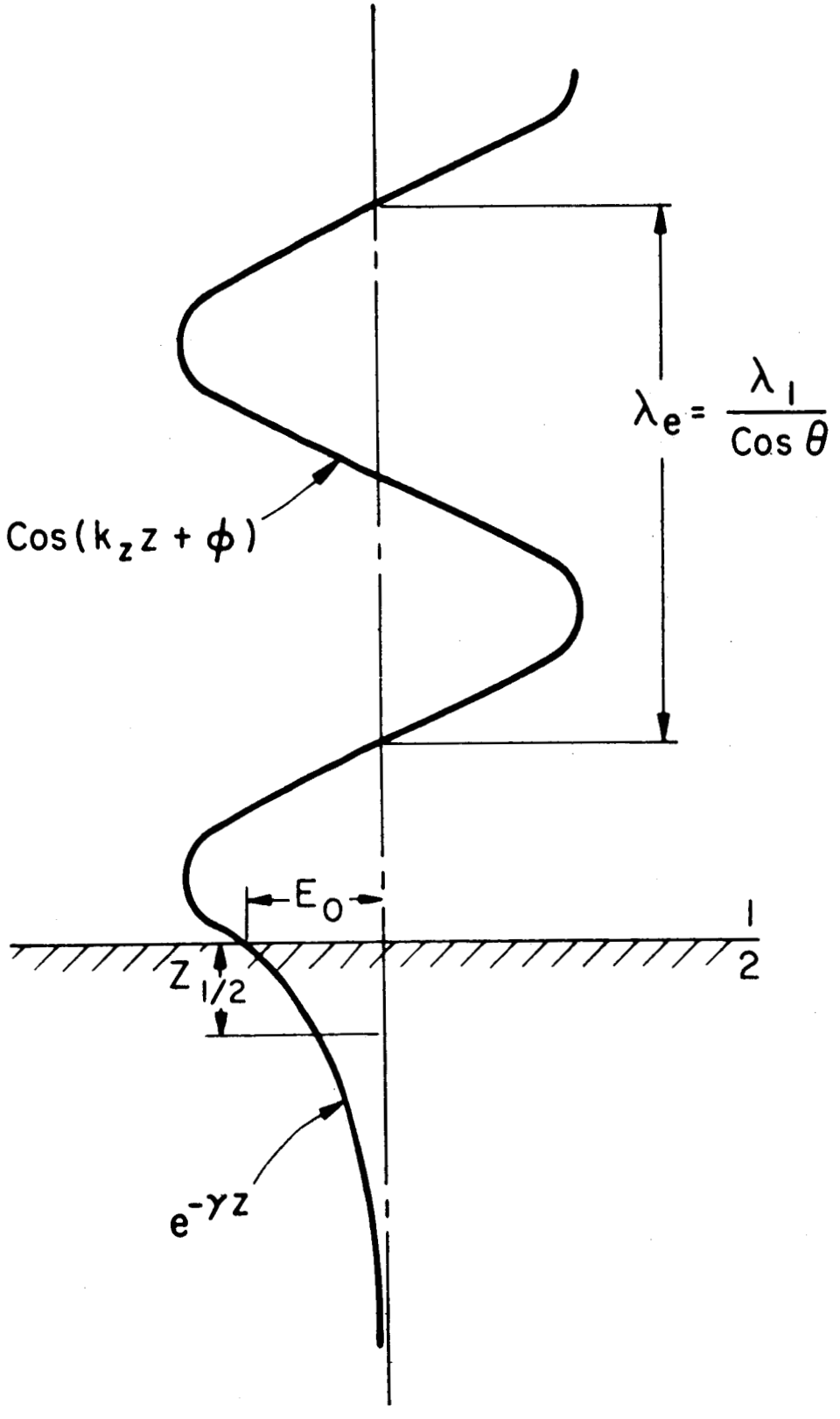

Figure 2: Standing Wave Pattern for Total Internal Reflection at Interface

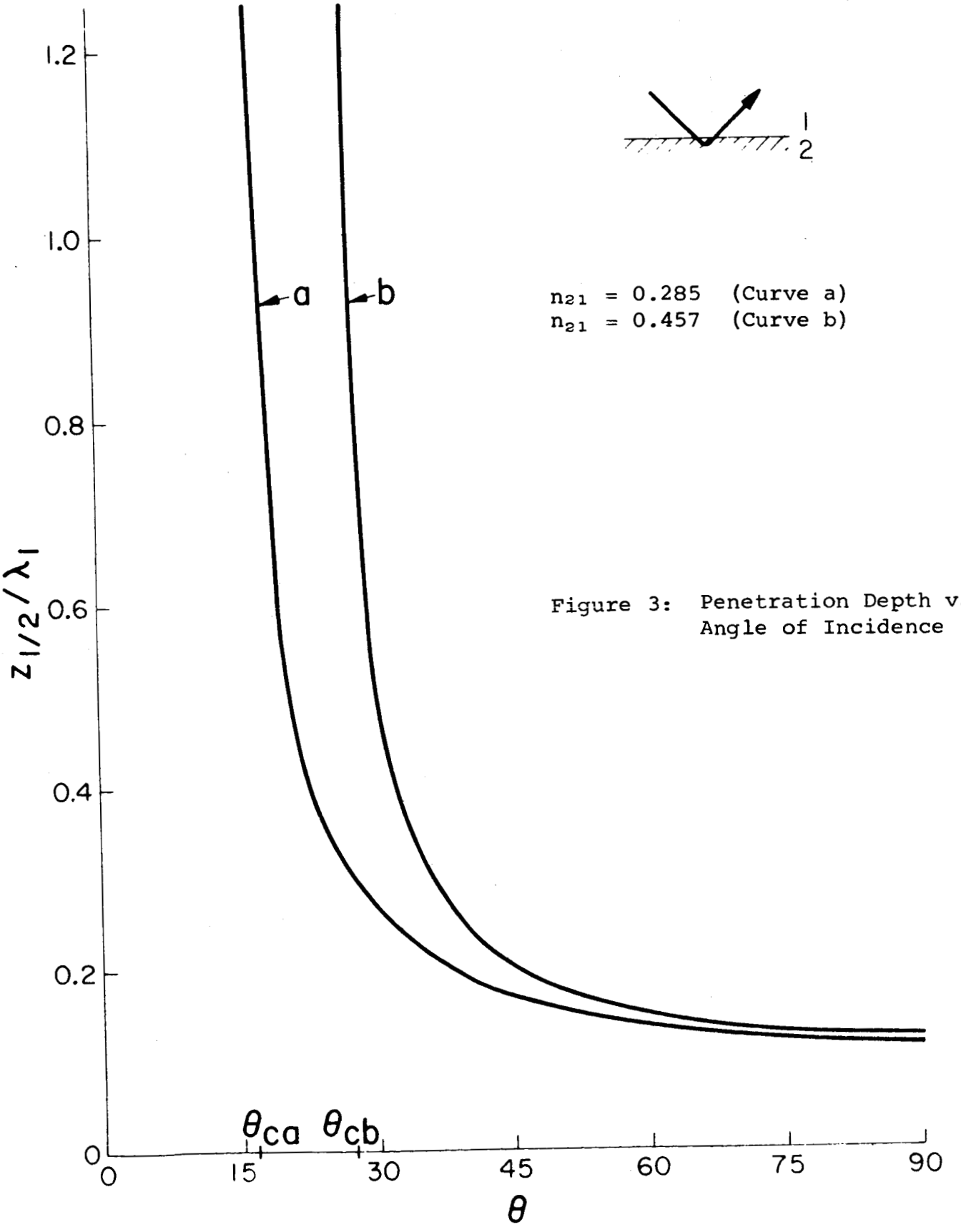

Figure 3: Penetration Depth vs Angle of Incidence

One important quantity for interactions with thin films on or near the surface is the electric field amplitude E_o at the surface. This has been calculated for the different polarizations and is shown in Figure 4 for unit incident amplitude. Here E_{yo} is the electric field vector perpendicular to the plane of incidence; it also represents the electric field amplitude for the light polarized perpendicular to the plane of incidence. For the light polarized parallel to the plane of incidence, it is more convenient to consider the components separately, i.e. E_{xo} and E_{zo}.

To determine the strength of interaction with a thin film placed on the surface, it is convenient to calculate the absorption parameter, a, which is defined as the amount of absorption per reflection for unit of incoming power. The reflectance R in the presence of absorption is then

$$R = R_o \quad (1-a) \simeq R_o e^{-a}$$

for weak absorptions. For films which are thin compared to the wavelength λ_1, the absorption parameter is found to be (Ref. 5):

$$a = \frac{n_{21}\ \alpha\ d\ E_o^2}{\cos\theta}$$

Here α is the absorption coefficient of the material on the surface and d is its thickness. The electric field amplitude E_o is always equal to or greater than $\cos\theta$; hence the interaction is greater the nearer to the critical angle the measurements are made. It should be noted that the absorption is greater the closer the matching of refractive index of the cell to that of the film; i.e. $n_{21} \rightarrow 1$. In actual practice, many reflections are employed and the total absorption parameter is thus Na and the reflectance is given by

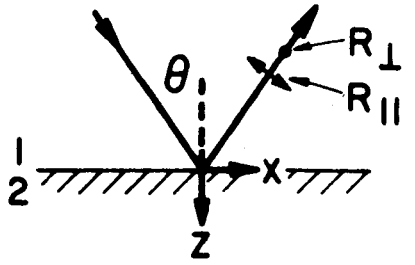

Figure 4: Calculated Electric Field Amplitude E_o for Unit Incident Amplitude vs Angle of Incidence θ at Totally Reflecting Interface for $n_{21} = 0.285$

$$R = R_o \ (1-a)^N \simeq R_o e^{-Na}$$

N is the number of reflections and is given by

$$N = \frac{\ell}{t} \cot\theta$$

where ℓ is the length of the cell and t is its thickness.

Since N rises sharply with decreasing θ, it would appear advantageous to make the cells from high index materials where the critical angle is small, and many reflections can be employed.

For angles below 45°, the aperture of the cell decreases, however, and thus there is a practical lower limit to the choice of angle of incidence. Once this lower limit is chosen to give as high a value of N as feasible, the formula for the absorption parameter suggests choosing a cell material so that the working angle is close to the critical angle when the degree of absorption per reflection is the greatest.

Measurements of the total absorption parameter Na vs angle of incidence for a thin film of polystyrene have been made and are shown in Figure 5. N has a value of about 100 at $\theta = 45°$. The sharp increase in Na with decreasing θ should be noted. This results from both an increase in N and a with decrease in θ. It should also be noted that, in agreement with theory, the absorption parameter is always greater for parallel polarization than for perpendicular. The strongest interaction can be achieved by orienting the dipoles normal to the surface because of the large values of E_{zo}. This might be done electrically.

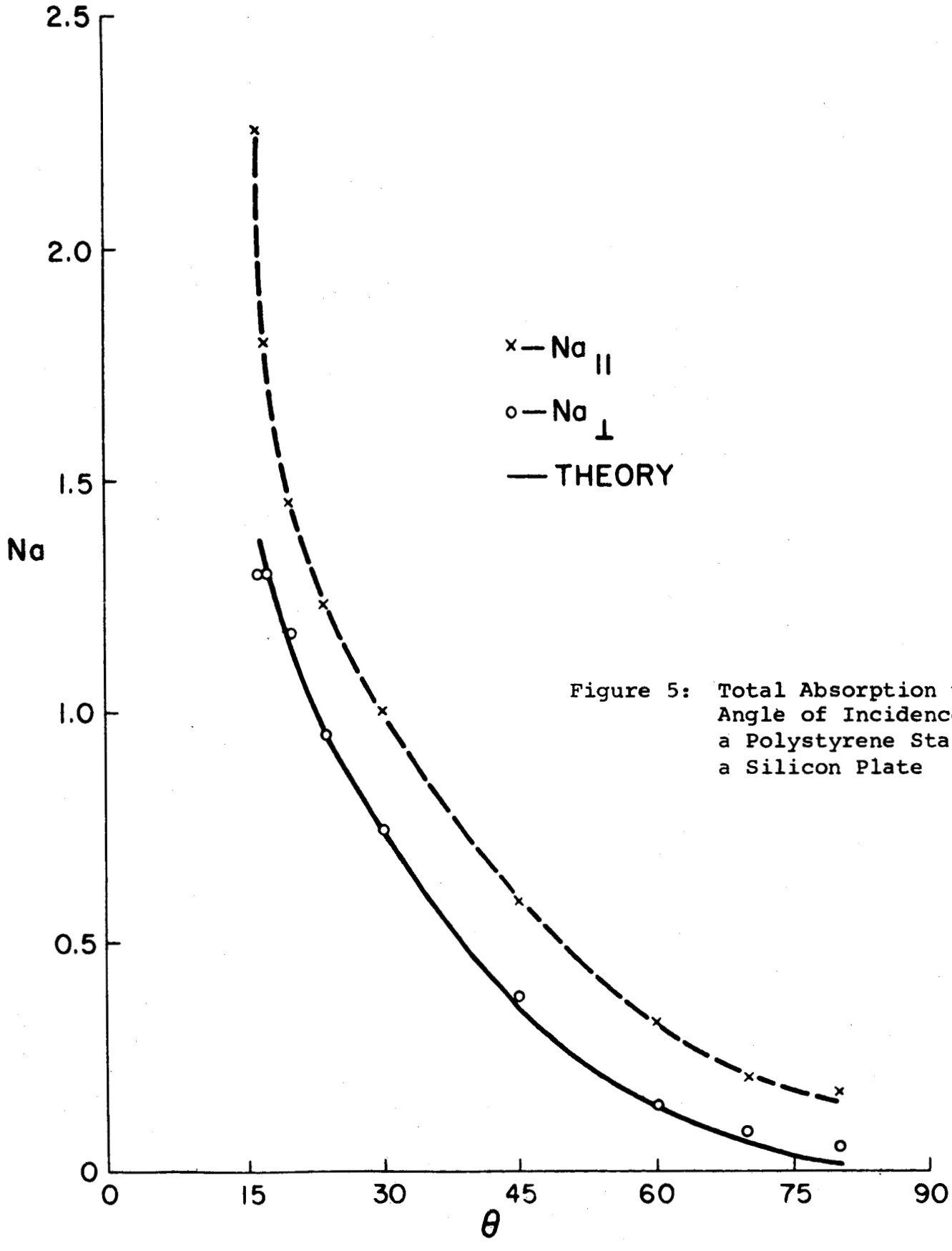

Figure 5: Total Absorption vs Angle of Incidence of a Polystyrene Stain on a Silicon Plate

The important advantages offered by the FMIR technique over conventional infrared absorption techniques are:

a) Sample preparation is easy. The sample to be studied need only be brought to within a penetration depth of the FMIR cell. For highly absorbing samples it is not necessary to prepare thin films or powder pellets as is done in conventional transmission spectroscopy. The rather tedious preparation of specularly reflecting surfaces is not required as in conventional reflection spectroscopy. Therefore, the sample may be analyzed in its natural state.

b) The bothersome interference phenomenon associated with films (liquid or solids) in conventional spectroscopy is absent.

c) The optical constants n and k of the sample in the vicinity of absorption bands can be measured. Measurements made for angles of incidence near the critical angle qualitatively resemble the mirror image of the dispersion in the refractive index n, while measurements made far from the critical angle closely resemble the absorption constant k. These measurements can be combined to precisely determine n and k.

d) Trace amounts of infrared absorbers can be detected, because the material to be studied can be efficiently placed on the FMIR cell. As a result, less material is required to obtain a spectrum than in conventional techniques.

e) Spectra of monolayer films can be obtained. Since hundreds of reflection (samplings) can be employed, the spectra of films, one monolayer or less in thickness, can be obtained. This multiple sampling feature also allows investigation of dispersed samples, e.g. powders.

f) The contrast of the spectrum obtained can be controlled by controlling the angle of incidence and the number of reflections.

g) Light scattering by powder samples is absent.

2. FMIR Cells. The type of internal reflection cell employed has a considerable bearing on the ease with which measurements can be made. Fahrenfort (Refs. 2, 3) has used a cell in the form of a hemicylinder for one reflection and a modified hemicylinder for as many as five reflections where the angle of incidence could be adjusted over a certain range. Harrick (Refs. 1, 4, 5) and others (Refs. 6, 7) have employed thin flat plates where up to 500 multiple reflections occurred between the plane-parallel surfaces; the cells were operated at a predetermined angle of incidence.

a) Single-Pass Cells. In single-pass cells, the entrance and exit windows are located at opposite ends of the plate. After the light is introduced into the cell at the entrance window, it is propagated down the length of the cell by means of multiple internal reflection from opposing plane-parallel surfaces - emerging from the exit window at the opposite end. Even though the plate thickness is large compared to the wavelength of the light employed, single-mode excitation is achieved because of the well

defined angle of incidence.

b) Double-Pass Cells. Figure 6 shows some double-pass cells. Here the light beam enters and exits from the same end of the cell. The light is propagated down the length of the cell by multiple reflection from opposing plane-parallel faces, is totally reflected at the far end, and then returns and emerges from an exit window located near the entrance.

Except for an angle of incidence of 45°, the angle of incidence for the reflection at the far end will, of course, be different - namely, the complement of the angle of incidence on the side. If there is concern that this may lead to a broadening of the absorption band, the end of the cell can be metallized or masked so that the reflection here will not play a part in the absorption. Because the angle of incidence at the end of the cell is the complement of the angle on the sides, the range of angles of incidence which can be employed is from the critical angle θ_c to $(90-\theta_c)$; for single-pass cells the range is θ_c to 90°.

Figure 6a shows such a double-pass cell designed for a predetermined angle of incidence and a specific number of reflections. The structure shown in Figure 6b, on the other hand, permits an adjustment of the angle of incidence as well as the number of reflections but only for a few specific angles of incidence; this is because the exit and entrance beams must pass through a common pivot point. When the angle of incidence is changed, the path

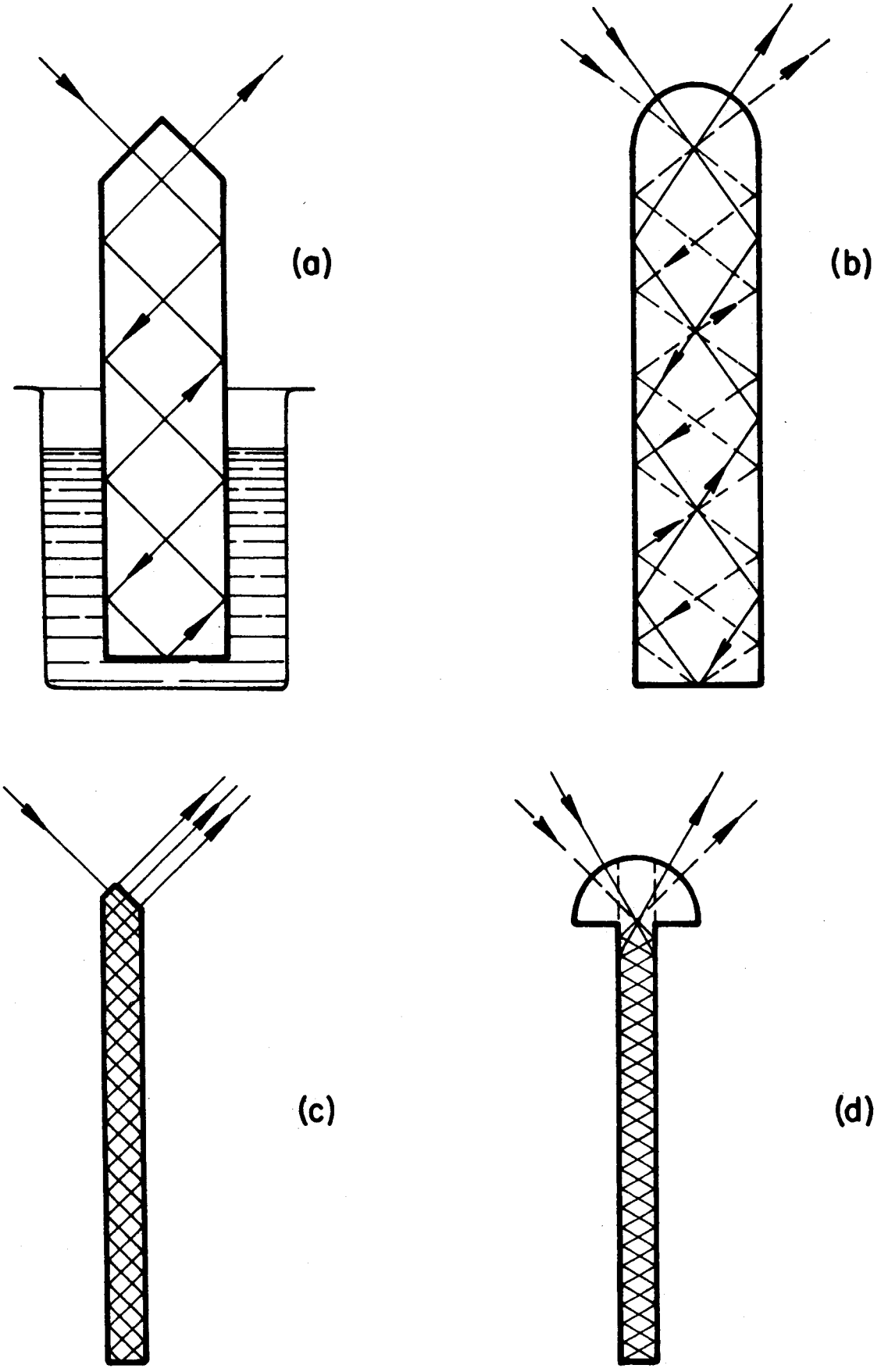

Figure 6: Double-Pass Multiple Reflection Cells

length in the cell changes, thereby altering the location of the external focus. This can be compensated for either by separate manual adjustment or a direct coupling to one of the mirror settings.

For a structure similar to that shown in Figure 6a, 50% of the emerging radiation will be directed back toward the source. This loss can largely be eliminated by making the entrance window smaller than the exit window, as shown in Figure 6c. If it is desired to vary the angle of incidence continuously, the structure shown in Figure 6d can be used with, of course, a 50% loss in light intensity.

3. Cell Preparation. There are a number of infrared transparent materials from which cells may be constructed (see Table 1). High index materials have the advantage that there is a wide choice in angle of incidence, and thus it is possible to employ many reflections when the cell length is limited. It is preferable to work with reflections from plane surfaces because the optics are then simplified.

When many reflections are employed, optically polished surfaces are required, since the reflection must be specular rather than diffuse. Light scattering not only causes a loss in sampling power, but makes balancing in double-beam arrangements more of a problem. Also, surface scratches induced through normal use lead to light scattering; when the power loss becomes excessive, the cell must be repolished or replaced.

Table 1: Parameters of Typical Infrared Transparent Materials for Cells

Cell Material	n	θ_c *	Useful Wavelength Range (microns)
Ge	4.0	14°30'	2 to 12**
Si	3.5	16°45'	1 to 7
KRS-5	2.4	24°40'	0.6 to 40
AgCl	2.0	30°	Visible to 20

* Critical angle for material/air interface

** Ge is transparent beyond 12 μ, but the transparency decreases markedly.

Smooth surfaces can be prepared by mechanical polishing. For certain experiments, however, the surfaces resulting from mechanical polishing are undesirable. Electro-polishing techniques recently developed for semiconductors (Ref. 8) are thus attractive. Other etching techniques, e.g. spin etch, are under investigation. The success of a thermal etch on silicon followed by annealing (Ref. 6) is also encouraging. With certain materials, cleaved surfaces might also be employed.

In cells designed for many reflections, the sampling surfaces must be plane-parallel to a high degree. If the surfaces are off parallel by 0.1°, for example, the internal angle of incidence will change by 10° after 100 internal reflections. The light beam will not reach

the exit window if it is directed from the thicker toward the thinner end of the cell and the working angle is less than 10° from the critical angle.

In general, it is preferable to cut and prepare the cell in one piece. When the structure becomes complicated, such as that shown in Figure 6d, it may be assembled from a number of pieces by optical contact along the dotted lines. Optical contact can readily be achieved between two surfaces polished flat to within one-twentieth of the wavelength of sodium light.

The desired angle of incidence is chosen according to the depth of penetration and electric field strength required in the rarer medium (Ref. 3). The angle of incidence also determines the number of reflections and aperture of the cell. These can be calculated from geometrical considerations and are shown in Figure 7.

The number of reflections is given by

$$N = \frac{\ell}{t} \cot \theta$$

for single-pass cells and is twice this for double-pass cells. Here ℓ is the length of the cell plate and t is its thickness.

For maximum aperture, the entrance and exit windows should be cut so that the light enters and leaves at normal incidence. This also eliminates polarization as well as dispersion due to refraction at the windows. The aperture is defined as that portion of window which transmits light internally reflected at the desired angle of

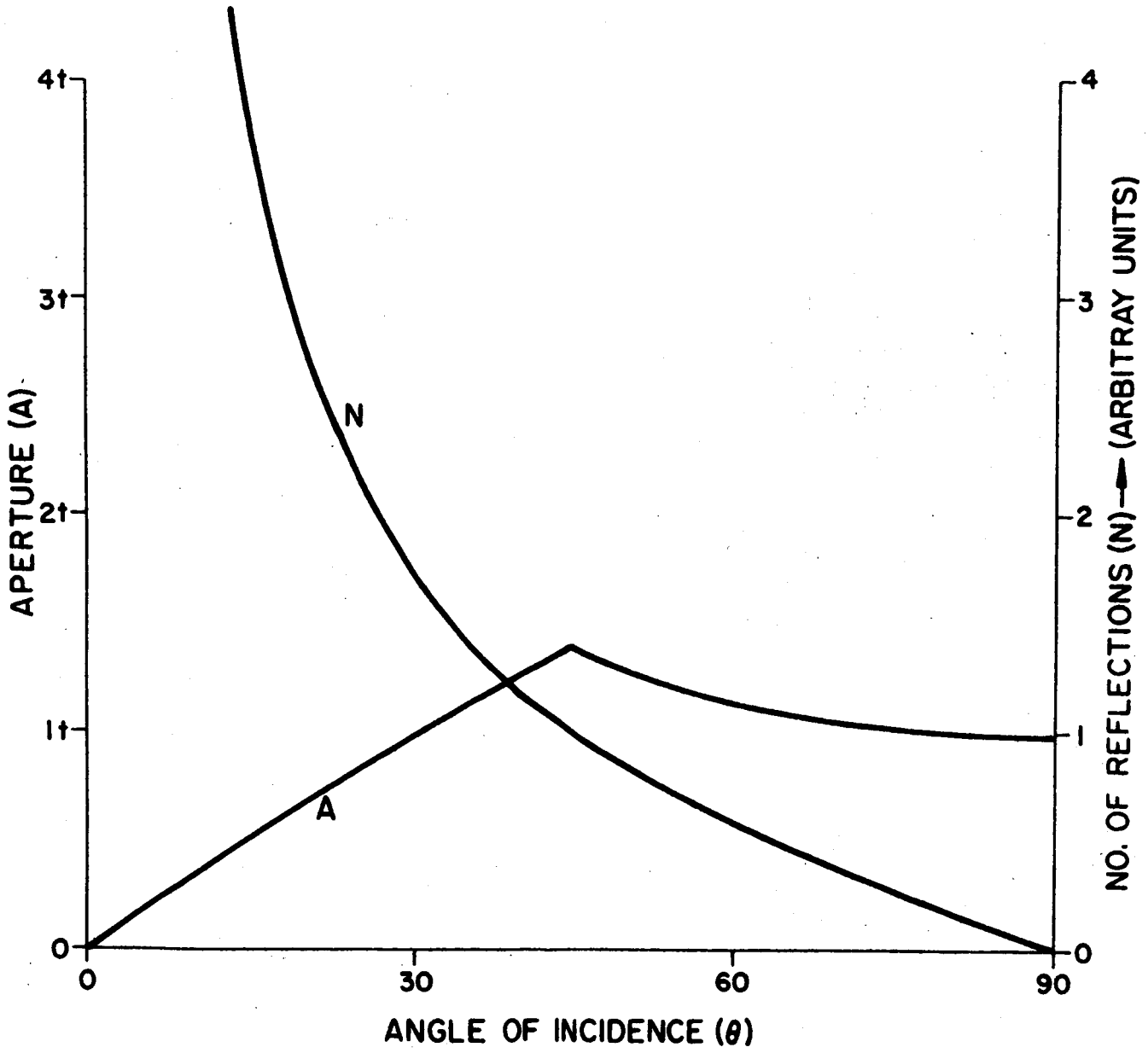

Figure 7: Number of Reflections and Aperture vs Angle of Incidence for Single-Pass or Double-Pass Multiple Reflection Cells

incidence. For angles of incidence less than 45°, only part of the bevel contributes to the aperture A:

$$A = 2\ t \sin\theta$$

For $45° < \theta < 90°$

$$A = t \sec\theta$$

For double-pass cells, A is the total aperture of the entrance plus exit windows, while for single-pass cells, A represents the aperture of either the entrance window or exit window. For double-pass cells, the total aperture remains constant regardless of how it is divided between the entrance and exit windows.

The dimensions of the cell are determined from the following considerations. The width of the cell is chosen to be equal to or greater than the height of the monochromator slit - e.g. 1 to 1.5 cm. The length-to-thickness ratio of the cell determines the number of reflections once the angle of incidence is selected. Previous cells used at Philips Laboratories were of thicknesses ranging from 0.25 to 5 mm and of lengths from 1 to 10 cm.

Typical dimensions of the optically finished cells used in this study were:

- Entrance and exit windows beveled for 45° angle of incidence
- Cell thickness 1 to 2 mm
- Cell height 20 mm
- Cell length 55 mm

Cells constructed from highly transparent material, with highly polished plane-parallel surfaces, transmitted close to theoretically expected power even for hundreds of reflections; the principal losses were due to reflections at the entrance and exit windows.

3.1.2 Instrumentation.

1. Optics. The cells shown in Figure 6 can be used in conjunction with any infrared spectrometer with the addition of suitable transfer optics. Since the sampling space provided in many spectrometers is often inadequate, it is desirable to either extract the monochromatic light beam from the spectrometer and work with external optics, or to modify the source optics of the spectrometer. The latter was done in this experiment. By the introduction of plane mirrors, the slit image can be rotated so that the cells can be operated in a vertical position, i.e. dipped into the powder or liquid sample.

An optically balanced double-beam system (see Figures 8, 9) was fabricated which employed two double-pass crystals as reference and sample cells. The balanced arrangement was chosen because of the high sensitivity available; high gain narrow band amplifiers can be used since the unbalance signal is AC. Also, light source intensity fluctuations and atmospheric absorption bands are minimized.

In this system the light emanating from the Nernst glower source is alternately focused onto the entrance window of the reference and sample cells. This alternation of the beam between reference and

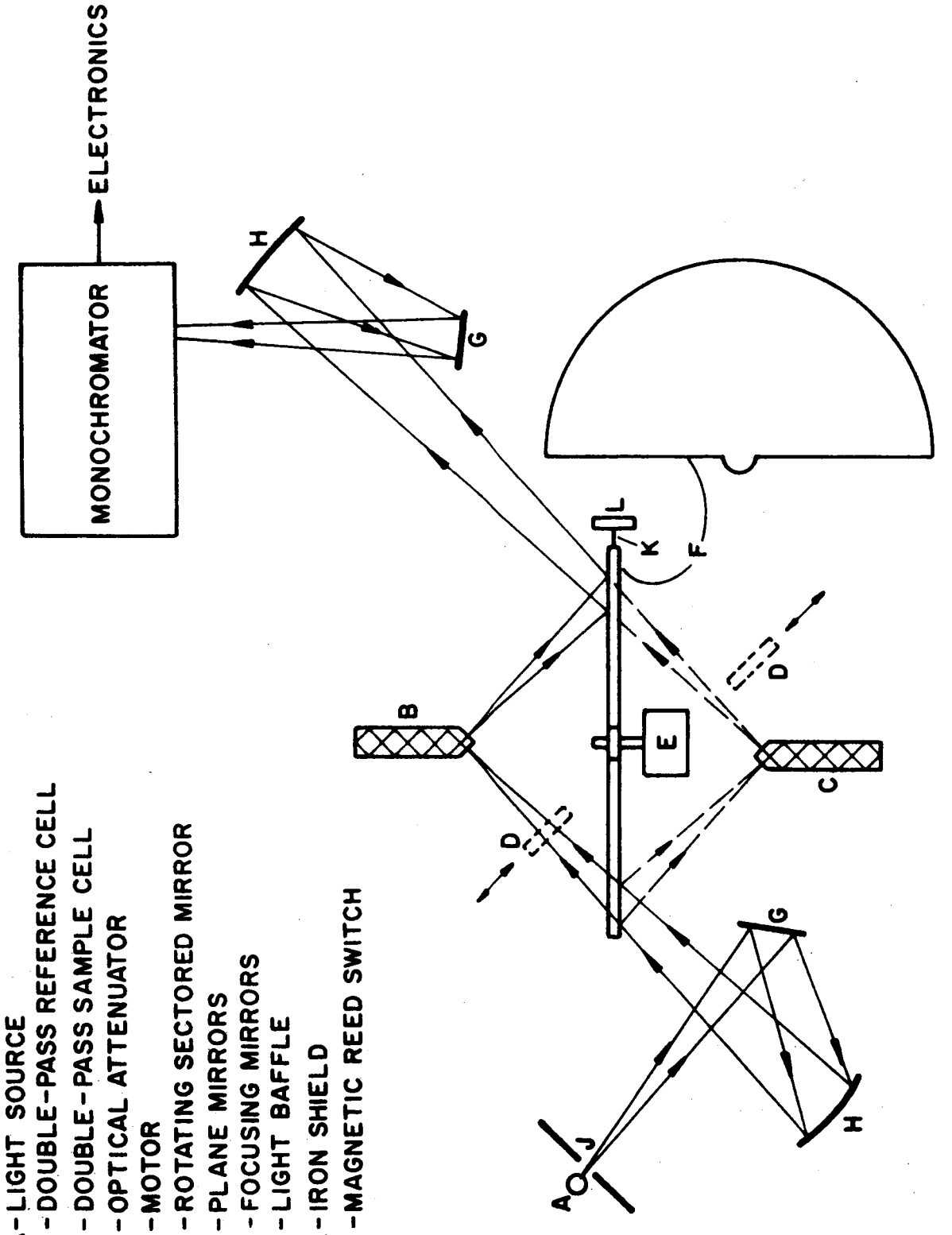

Figure 8: Schematic of Balanced Double-Beam System

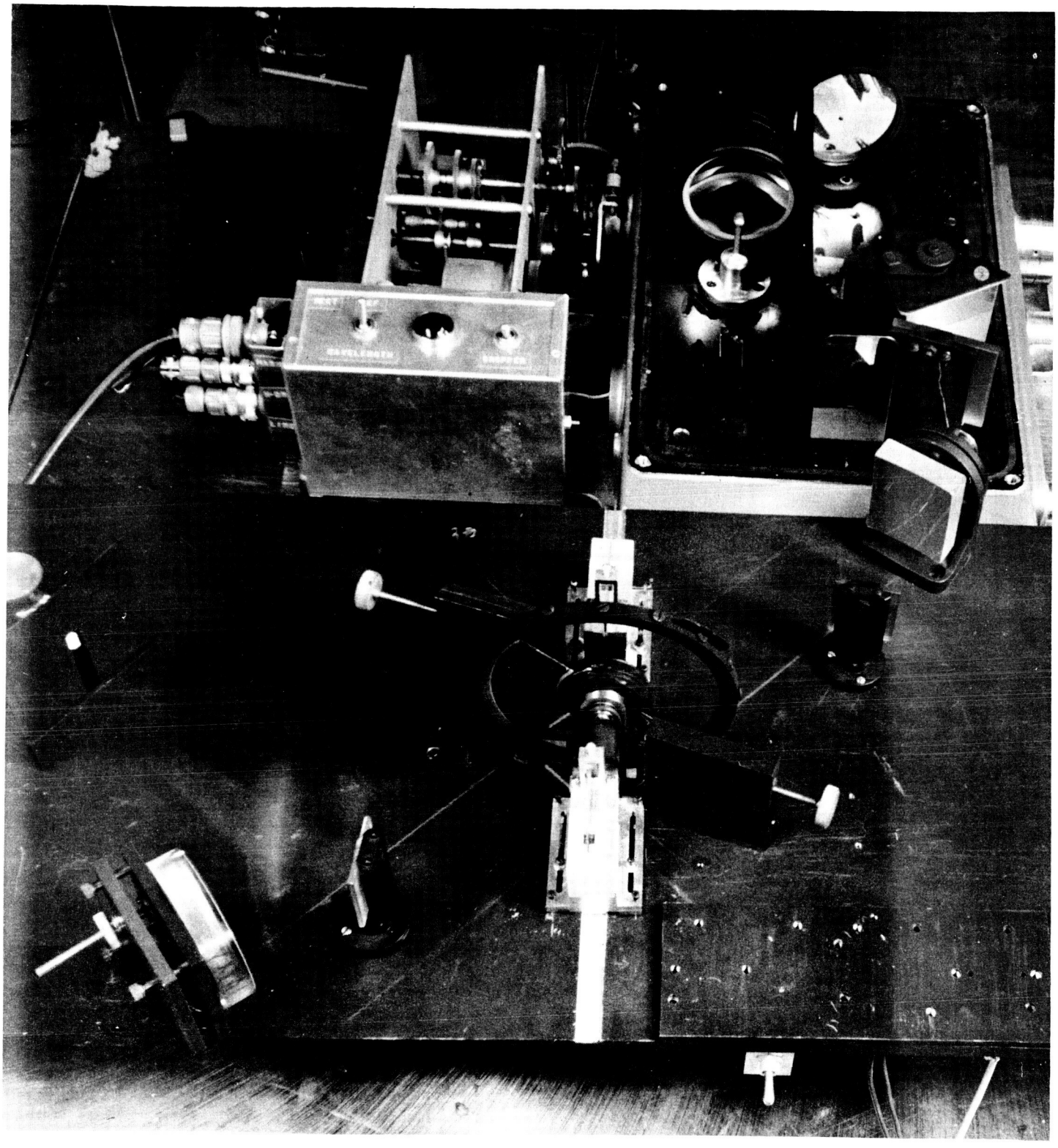

Figure 9: Balanced Double-Beam System

sample cells is accomplished at the rate of 12 cps by means of a single chopping mirror silvered on both sides. The mirror acts as a beam splitter and a beam recombiner. Due to mirror thickness, the sample cell is placed off axis. The recombined beam is focused onto the entrance slit of the monochromator (NaCl prism) and passed onto a thermocouple detector. Since the split beam travels equal paths through equal media, the effects due to atmospheric absorptions and absorptions common to the cell material are minimized.

In order to compensate for minor unbalances in the system due to differences in cell lengths, cell surface finish, etc., optical attenuators are placed in both the reference and sample light paths (see Figure 8, 9). However, an attenuator is only necessary in the path of the light beam passing through the more transparent cell. At the present time, balance is achieved at a single wavelength in the spectra by fixing the position of the attenuator; however, the use of servo-driven attenuators would allow balance to be achieved throughout the optical range of the instrument.

For any given slit width setting of the monochromator, more power was transmitted at the shorter wavelengths. This caused the absorption spectra to be distorted, with maximum signal and maximum signal resolution occurring at the shorter wavelengths.

Special cell holders were fabricated which permitted the cells to be rotated about a fixed pivot point, to be moved in line with point of focus of the convergent light beam, and to be tilted for

maximum illumination of the entrance window. The mirror is driven by a belt drive. An iron shield, which activated the magnetic reed switch generating the synchronous signal, was placed directly on the lucite mirror holder.

Some of the advantages of the balanced double-beam system are as follows:

a) No detector matching (sensitivity vs. λ) is necessary since there is only one detector. Changes in detector characteristics due to age, shock, ambient temperature, and deterioration of its window are the same for both light paths (sample and reference).

b) If present, naturally occurring bulk absorptions (molecular resonances in cell) are balanced out - provided the cells are at the same temperature.

c) Mirror and chopper are a single unit, thereby minimizing system vibration.

d) System uses power emanating from the source 100% of time; it does not lose 50% of the power as would a system employing an opaque mechanical chopper.

e) Effect of changes in refractive index of cell as a function of wavelength is eliminated.

f) Since the output of the optical system is AC difference

signal (unbalance signal), a high gain narrow band AC amplifier can be used.

g. The balanced output is independent of variations in light source intensity with wavelength.

2. Cell Material. A number of infrared transparent materials were obtained from commercial sources - germanium, silicon, KRS-5, silver chloride, IRTRAN II, IRTRAN IV, and gallium arsenide. In all cases except silver chloride, these crystals were fabricated into double-pass cells; the entrance and exit windows were angled at 45°, and the collecting surfaces were polished to an optical finish.

a. Silver Chloride Cells. Although the AgCl crystal, obtained as rolled stock, is transparent throughout the region of interest, its softness makes it highly susceptible to scratches and other surface deformations induced in the rolling process and in use.

b. IRTRAN II and IRTRAN IV Cells. These cells, made of pressed materials, do not exhibit uniform optical characteristics from cell to cell. The scattering of light due to the granular nature of the cell causes excessive loss of sampling power. The use of IRTRAN cells in a balanced system, which requires matched pairs of cells, would require time consuming effort to select matched pairs; this is due to the present state of the art of crystal manufacturing.

c. KRS-5 Cells. These cells are transparent to infrared radiation over a wide range of wavelengths but are susceptible to

surface scratches because of the crystal's softness. Scratching occurred when the cells were cleaned by brushing with soft cotton. The mixed crystal composition of KRS-5 (TlBr-TlI) is such that the composition of the cell's surface changed (preferential leaching of the thallium compounds) when the cell was cleaned with wet organic solvents or mild detergents in aqueous solution. This resulted in increased scattering of the internally reflected radiation, with subsequent loss in sampling power.

d) Germanium and Silicon Cells. These cells exhibit long life and ruggedness and can be readily cleaned by utilizing camel hair brushes, air brushes, and/or mild detergent washes.

Silicon exhibits high transparency in the 1 to 6 μ wavelength range and beyond 20 μ. The transparency of the germanium cells is rather high from 2 to 12 μ, and there are no losses due to molecular resonance absorption in this region. Beyond 12 μ, however, the transparency of germanium falls off due to lattice bands and surface oxidation; two broad absorption bands were noted between 12 and 14.5 μ.

e) Gallium Arsenide Cells. Preliminary experiments on high resistivity (compensated) GaAs cells indicate high transparency over the 0.9 to 15 μ wavelength region defined by the monochromator. This material has physical characteristics similar to that of silicon and germanium. It may prove to be useful as a cell material. It is known that high resistivity GaAs is transparent beyond 15 μ.

3. Cell Balance. In the balanced arrangement, it is desirable that the transmission characteristics of both crystals be identical over the entire transmission range of interest. This is possible since the cells are made from materials (silicon and germanium) from which homogenous ingots can be prepared and the surfaces of the cells can be polished consistently to the required specifications.

The intensity of the naturally occurring molecular resonance absorptions of each crystal must be identical in magnitude in order to prevent an imbalance in the optical system. This constraint dictates the use of crystals of identical length so that the same optical path lengths are traversed. The same number of internal reflections (samplings of the surface) should be taken, for if one crystal were longer for a given thickness, it would naturally sample more of the background interfering agents - e.g. condensed H_2O, hydrocarbons, etc. The presence of appreciable amounts of such contaminants are not expected in a lunar environment.

4. Electronics. The light power incident upon the thermocouple detector in the monochromator varies between two discrete levels -- the high level being the absorption spectrum of the reference cell crystal and the low level being the absorption spectrum of the sample cell crystal plus the powder sample. Hence, the incident power on the thermocouple varies in "square wave" fashion, generating a square wave voltage across the thermocouple. The amplitude of this square wave is a direct function of the difference of absorption between the two cells. The frequency of this square wave is the same as the optical chopping frequency (12cps). This signal is the in-

formation input to the system electronics amplifier.

A second voltage signal was generated by the chopping system for synchronization purposes. This was done by a magnetic reed switch mounted near the periphery of the mirror and an iron shield mounted on the periphery of the mirror. The magnetic switch is activated by the shield once each revolution. Thus, pulses are generated at the chopping frequency rate and are, therefore, synchronized with the optical chopper and the information signal. This synchronization signal is applied to the synchronous detector in the amplifier.

A block diagram of the system electronics is shown in Figure 10. The system consists of a high gain amplifier, synchronous detector, panel meter, and X-Y pen recorder. The recorder generates a plot of absorption versus wavelength while the panel meter, a zero-center microammeter, indicates the magnitude of the absorption (unbalance). Initially, before a sample is introduced onto the sample cell, the optical system is adjusted to yield a null (zero deflection on panel meter and recorder).

The amplifier used was a Philips Selective Voltage Amplifier. It is a high gain (186db maximum) narrow band (0.35 cps maximum) selective amplifier centered at 12 cps. The information signal is amplified andapplied to one input of a synchronous detector within the amplifier. The synch signal is applied to a second channel within the amplifier where it is shaped and phase adjusted; it is then applied as the drive signal to the synchronous detector. The output of the detector is a DC voltage whose level is a direct function of the amplitude of the information signal. The polarity of this voltage appearing across the zero-center panel meter and the recorder output jack is a function of the relative phase of the in-

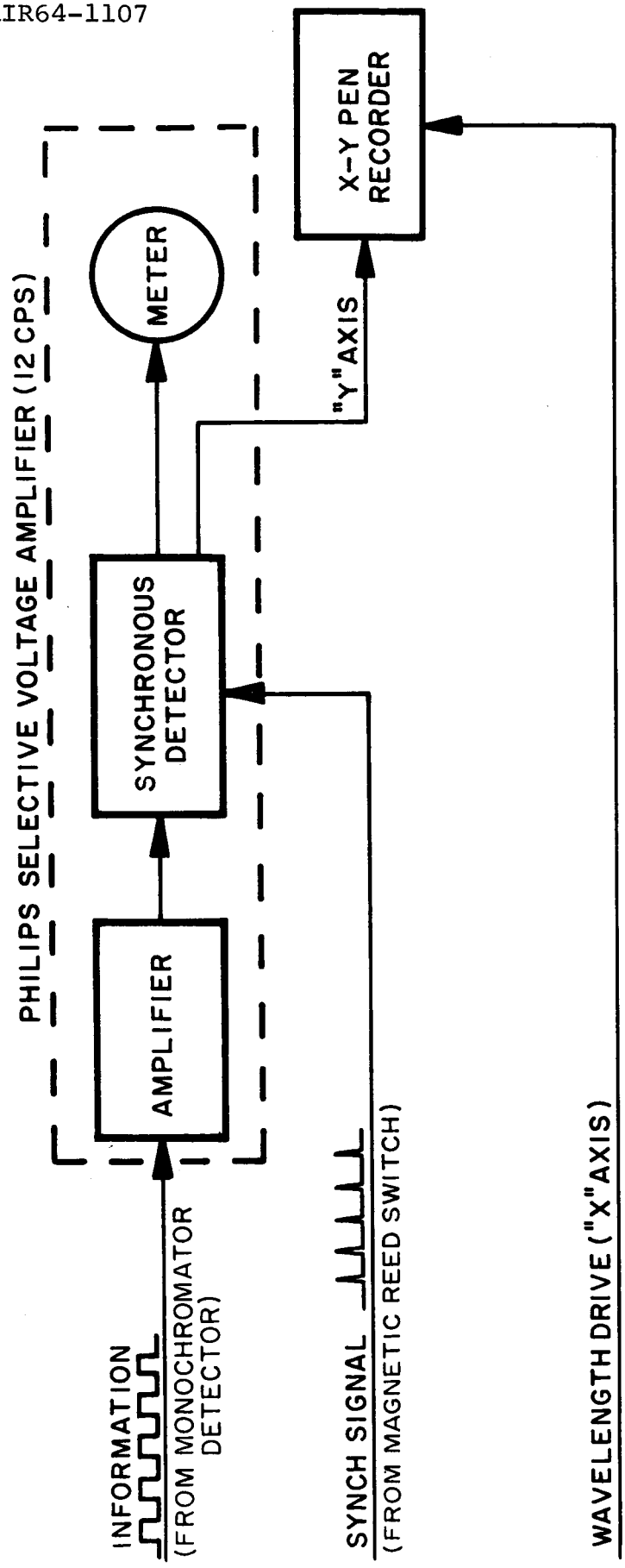

Figure 10: BLOCK DIAGRAM OF SYSTEM ELECTRONICS

formation and synch signal. The maximum gain from signal input to the meter is 186db; the maximum gain from the input to the "recorder output" terminal is 130db.

The X-Y pen recorder used was a Moseley 135M. This recorder has its own internal amplifier whose gain and time constant are variable. By measuring the "noise deflection" of the recorder and using the gain figures of the recorder and amplifier, it was determined that the equivalent noise input was in the order of 10^{-9} volts. For a poly-vinylidene-chloride (saran) deposit, this corresponds to a minimum detectable signal which is equivalent to < 5% absorption at 9.5 μ (Ref. 9).

3.2 Sample Preparation

3.2.1 Particle Separation

Lo-Micron Silica powder of maximum particle diameter 43 μ was obtained from A. D. MacKay Inc. The powder consisted of ground naturally occurring quartz which is not pure SiO_2, since it contains mineral impurities of low metal content, i.e. approximately 50% kaolinite clay as determined by X-ray diffraction analysis at Philips Laboratories.

The powder was separated by means of a Roller Particle Size Analyzer into particle size groupings of 0-3.5 μ, 3.5-5 μ, 5-10 μ, 10-20 μ, 20-30 μ, and 30-43 μ. The analyzer, a single stage air elutriator manufactured by the American Instrument Co., separates finely divided material according to particle diameter.

The instrument performs the separation as follows: A sample of dried material to be separated is placed in a sample tube. Pressure regulated air is then passed through a nozzle into the sample tube. This steady stream of air carries particles of the powder sample into a settling chamber mounted above and connected to the glass sample tube. As the air stream with its entrained particles enters the settling chamber, it passes through a diffuser section, expanding in cross-section to the area of the actual settling region. In expanding, it assumes a definite linear velocity. The force exerted by the air stream will be great enough to carry particles of a given diameter, and all particles smaller in diameter, upward through the settling chamber. Particles larger than

the given diameter will fall back, against the force of the air stream, into the glass sample tube. The upper portion of the settling chamber diminishes in cross-section as the top is approached, so that the air stream velocity increases at it carries the particles out of the chamber, through a "gooseneck" tube, and into a collecting thimble. The thimble is made of porous material enabling it to pass the air stream while retaining the particles.

The principle of the Roller Particle Size Analyzer is based on Stokes' Law, where the velocity V of a spherical particle falling freely in a viscous medium is expressed by

$$V = \frac{gd^2 (\rho - \rho_a)}{18 \eta} \quad \text{cm/sec} \qquad (1)$$

where d = diameter of particle,

g = 980 cm/sec^2,

η = viscosity of the fluid medium (1.82×10^{-4} poise for air at 20°C),

ρ = density of particle,

ρ_a = density of fluid medium

If the density of the air is neglected, Stokes' Law reduces to

$$V = 29.91 \times 10^{-4} \rho \, d^2 \text{ cm/sec}, \qquad (2)$$

where the particle diameter is expressed in microns.

The required air-flow rate F on a volume basis, is the required

air velocity multiplied by the cross sectional area of the settling chamber being used, or

$$F = \frac{V\pi D^2}{4} \text{ cc/sec} \quad \text{or} \tag{3}$$

$$F = 47.1\, VD^2 \text{ cc/min} \tag{4}$$

where D = settling chamber diameter (cm)

Substituting the expression for V into the equation for F, one obtains

$$F = 0.1409 \times 10^{-3}\, d^2D^2 \text{ liters/min,} \tag{5}$$

where ρ was taken as 2.65 gm/cm^3 for silica.

A silica separation schedule is shown in Table 2.

3.2.2 Preparation of Rough Solid Samples.

Samples of fused quartz plate and soda glass plate were frosted by grinding them with a 240 mesh alumina/water mixture until the plates became diffuse reflectors.

Table 2: Silica Separation Schedule

Maximum Particle Diameter of Fraction (microns)	Chamber Diameter (inches)	Airflow (liters/min)	Orifice Diameter (inches)	H_2O Kanometer Pressure (cm)	Nozzle Diameter (inches)	Hg Manometer Pressure (cm)	Corrected Airflow (liters/min)	Time of Run (minutes)	Initial Hg Recording for h_h
3.5	9	2.5	.066	3.3	.038	.3	3.31	90	1.35
5	9	5	.066	11	.046	.6	11.1	60	1.75
10	4 1/2	5	.066	11	.046	.6	11.1	45	1.7
20	2 1/4	5	.066	11	.046	.6	11.1	30	1.6
30	2 1/4	11	.120	3.85	.070	.65	3.88	15	1.9
40	1 1/8	5	.066	11	.046	.6	11.1	40	1.7

Note: Silica density = 2.65 grams/cm^3

3.3 Measurements

3.3.1 Absorption Spectra of Powder Samples.

Infrared absorption spectra were obtained of a number of silica and quartz samples by placing the powder samples in close contact with the germanium sample cell (see Figure 8). The samples investigated included 0-150 μ (100 mesh) and 0-300 μ (40 mesh) quartz powder, unelutriated Lo-Micron Silica powder (0-43 μ in diameter) and Lo-Micron Silica powder of particle diameters 0-3.5 μ, 5-10 μ, 10-20 μ, 20-30 μ, and 30-43 μ. A number of absorption spectra are presented in Figures 11 through 16; a plot of percent absorption vs wavelength for the 5-10 μ diameter Lo-Micron Silica powder is shown in Figure 17.

Owing to the spectral emission characteristics of the glower source, the 2 to 14.5 μ wavelength range was covered in three sections; this required readjusting the amplifier gain and monochromator slit width. Four runs were made, for each sample, over the entire range. They are as follows:

a. Zero level curve - represents the zero line obtained by blocking off the infrared power at the point of entrance of the light beam into the monochromator.

b. Balance curve - represents the "double-beam" trace obtained when the infrared power emerging from the reference cell is balanced against that emerging from the sample cell with no powder present.

c. Absorption curve - represents the "double-beam" trace with the sample (powder) in contact with the surface of the sample cell; this is the infrared absorption spectrum of the sample. It should be noted that this curve coincides with the balance curve in a number of specific regions, i. e. 2 to 7 μ, near 11 μ, and again beyond 13 μ -- indicating that there is no absorption or scattering occurring in these regions.

d. 100% absorption curve - represents the power level and was obtained by blocking off the light emerging from the sample cell. The amplifier gain was adjusted for these runs in order to keep the curves on scale. The bands appearing beyond 11 μ are lattice and/or germanium oxide bands which are characteristic of the cell material. It should be noted that the centers of these bands do not occur at the same wavelengths as the centers of the molecular resonance absorption bands of the powder sample. For clarity, to avoid clutter, the 100% absorption curve has been removed from many of the spectra.

The vertical marker pips on the spectra relate the wavelength drum settings on the Perkin-Elmer spectrometer to actual wavelengths in microns via a calibration chart.

The useable optical range of the FMIR technique is determined by the transmission range of the cells and the dispersing media (visible to 15 microns for NaCl prism), and the resolving power of the system is affected by the slit width. Since the monchromator used to obtain the FMIR spectra was not equipped with a slit width drive, it was not possible to maintain constant light power at all wave-

lengths in any single scan. The absorption bands contained in the FMIR spectra were therefore, slightly distorted. The total excursion of an absorption band, from 0 to 100% absorption, varied in length (Y axis) through the wavelengths covered; the excursion was greater on the short wavelength side, since the intensity of the radiation increased with decreasing wavelength.

The 2 to 7 μ wavelength range was scanned at a slit width setting of 200 μ, the 7 to 12 μ range at a 600 micron slit width setting, and the 12 to 14.5 μ range at a 1000 micron slit width setting.

The quantities of the material (sample volume) investigated were determined by the total amount of material in close contact with the cell. Since packing fraction is a function of particle size, sample volume increases with decreasing particle size, for equal cell surface area exposure. In the present investigation, the double-pass cells were used in a horizontal position as shown in Figure 9. A small lucite container was provided to hold the powder around the cell. In order to increase the packing fraction, the powders were pressed lightly against the cells; approximately 75% of the cell surface area was covered. The effect of particle size on absorption is seen in Figure 18 which shows increased absorption for the smaller particle diameters at all absorption band wavelengths.

The high spectral contrast of the obtained patterns is evident. For particles sizes ranging from 0 to 43 μ in diameter, no loss of sampling power due to scattering was observed in the 2 to 12 μ

wavelength range. No decrease in sampling power as a function of wavelength was noted with this particular experimental setup.

For the Lo-Micron Silica samples, absorption bands were noted at wavelengths of 8.6, 9.0, 9.7, 9.9, 10.7, 10.9, 12.5, 12.8, and approximately 14.2 μ. The measured half-widths of the composite absorption band (8.6 to 9.9 μ band) of the Lo-Micron Silica powder are 30, 32, 32, 33, 30 and 31 millimeters for the spectra of the 0-3.5, 3.5-5, 5-10,10-20, 20-30, and 30-43 μ particle size groupings, respectively. This indicates that there is no band distortion.

The positions of the absorption band peaks obtained by FMIR Spectroscopy for Lo-Micron Silica (see Table 3) agree with the positions of the peaks obtained by Lyon (Ref. 10 and Figures 19, 20). The appearance of extra peaks in the 8 to 14.5 μ wavelength range was due to the kaolinite component of the powder. An O-H stretch band observed at 2.8 μ was further evidence of the presence of kaolinite.

3.3.2 Absorption Spectra of Rough Solids

Figures 21 and 22 are the absorption spectra of frosted fused quartz plate and frosted soda glass plate, respectively. The spectra were obtained in the same manner as were those of the powders. The quartz plate has absorption bands at wavelengths of 8.2, 8.8, 9.55, and 12.5 μ; the glass plate has absorption bands at wavelengths of 9.15, 9.9 and 12.5 μ. The absorption bands are rather broad.

Table 3: Position of Silicate Absorption Band Peaks in 8 to 14.5 μ Range For Spectra Obtained by Conventional Spectroscopy and FMIR Spectroscopy.

Conventional Spectroscopy			FMIR Spectroscopy
Powdered Quartz (KBr Pellet) (microns)	Fused Silica (microns)	Quartz* (microns)	Lo-Micron Silica (microns)
8.6	8.5	8.6	8.6
9.1	9.1	8.8	9.0
9.4	12.4	12.6	9.7
10.2	14.4	12.8	9.9
12.7		14.4	10.7
12.9			10.9
14.5 (approx)			12.5
			12.8
			14.2 (approx)

* The general assignments for quartz spectra peaks are 9.1 to 12.5 μ (Si-O stretch) and 12.5 to 16.7 μ (Si-Si stretch).

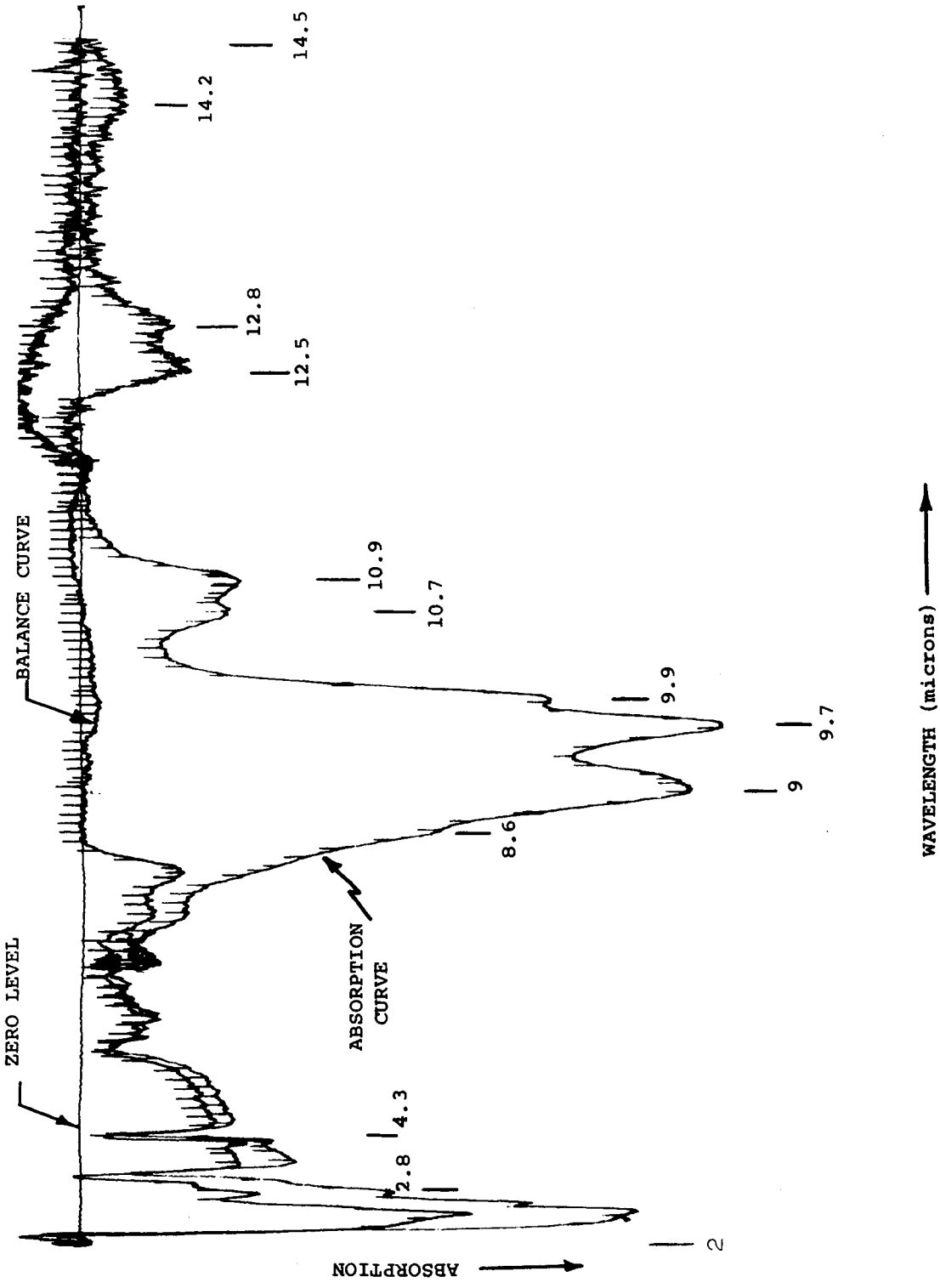

Figure 11: Absorption Spectrum of Lo-Micron Silica Powder (0 - 3.5 μ diam.)

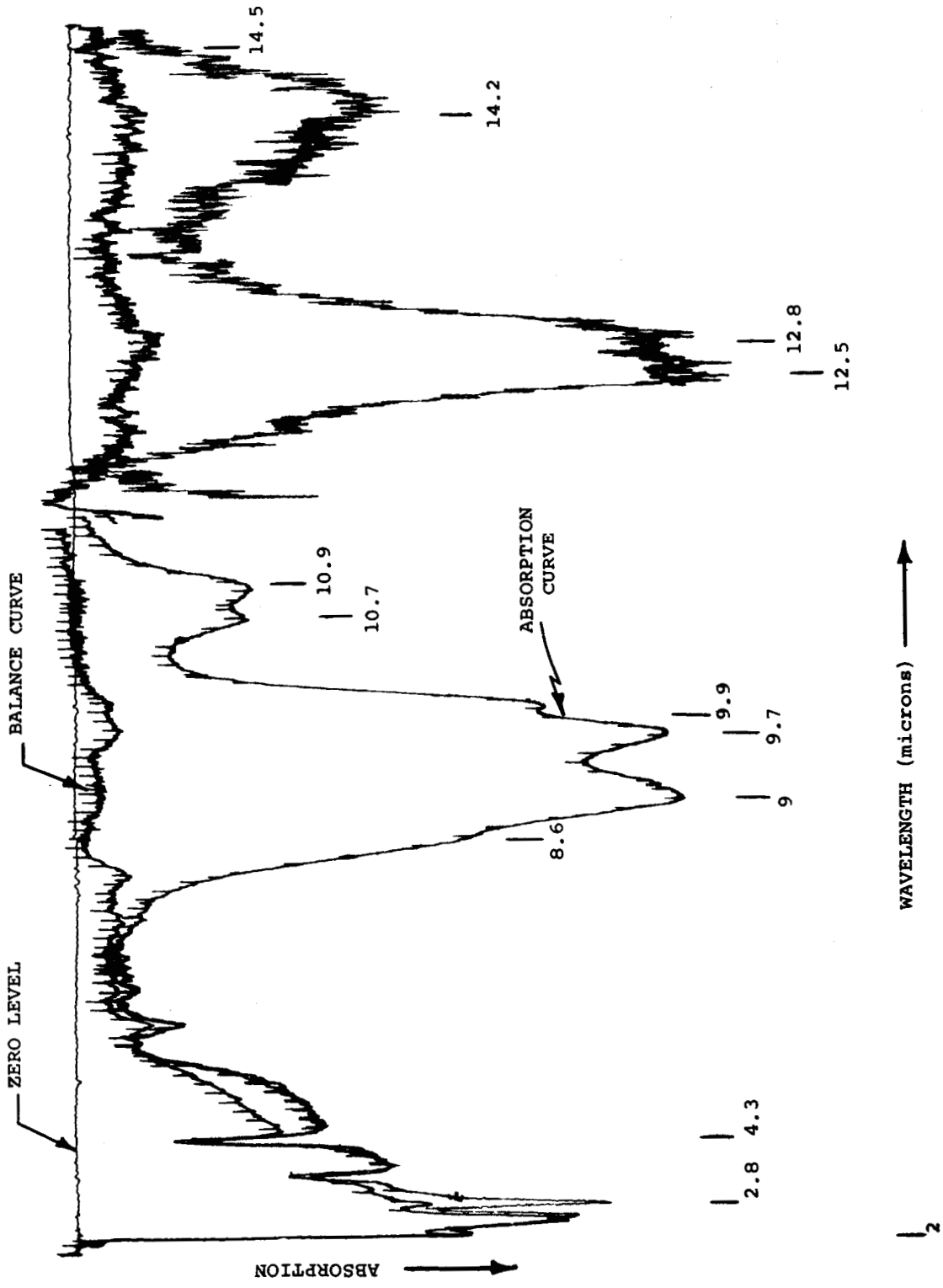

Figure 12: Absorption Spectrum of Lo-Micron Silica Powder (3.5 - 5 μ diam.)

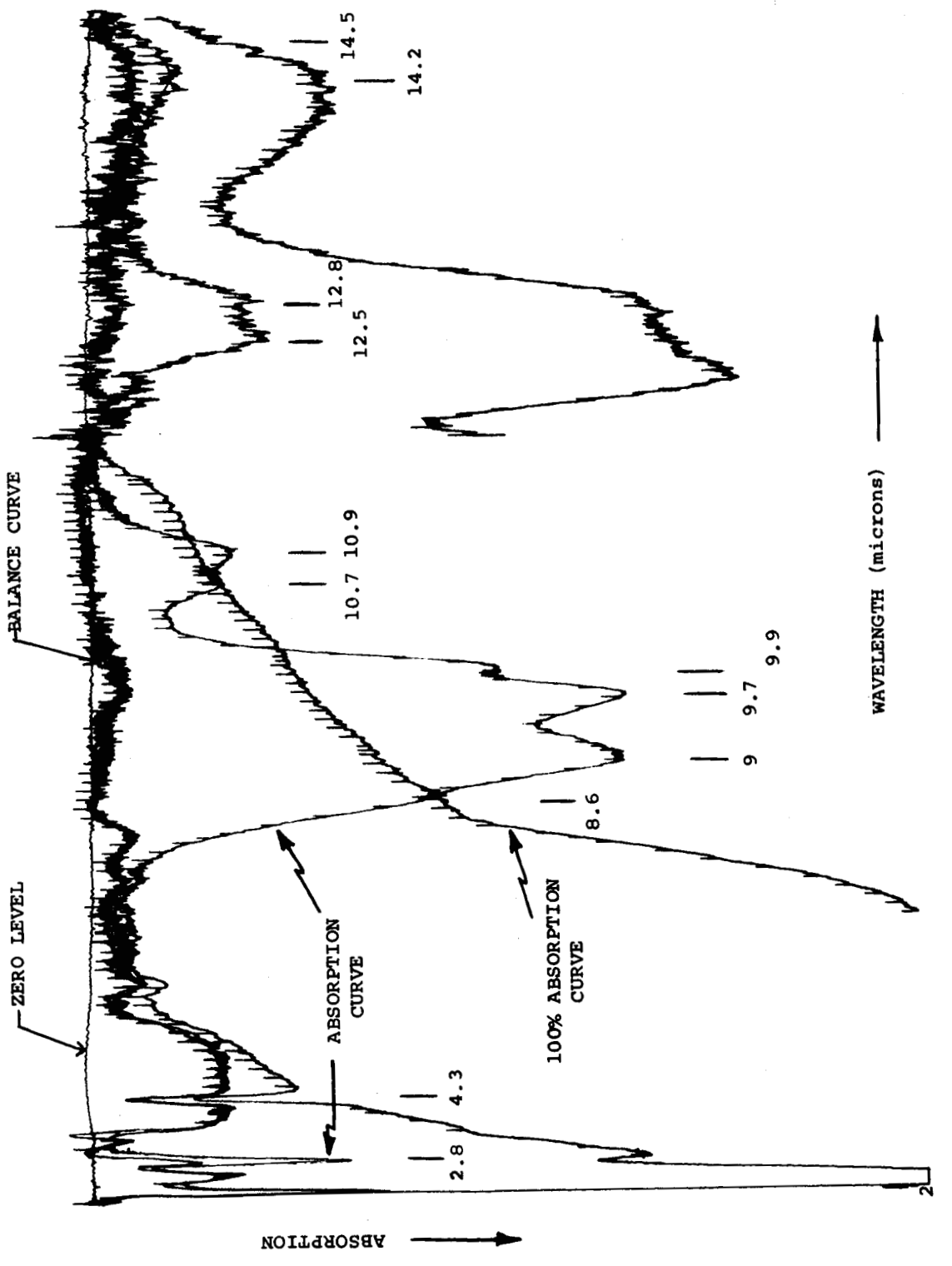

Figure 13: Absorption Spectrum of Lo-Micron Silica Powder (5 - 10 μ diam.)

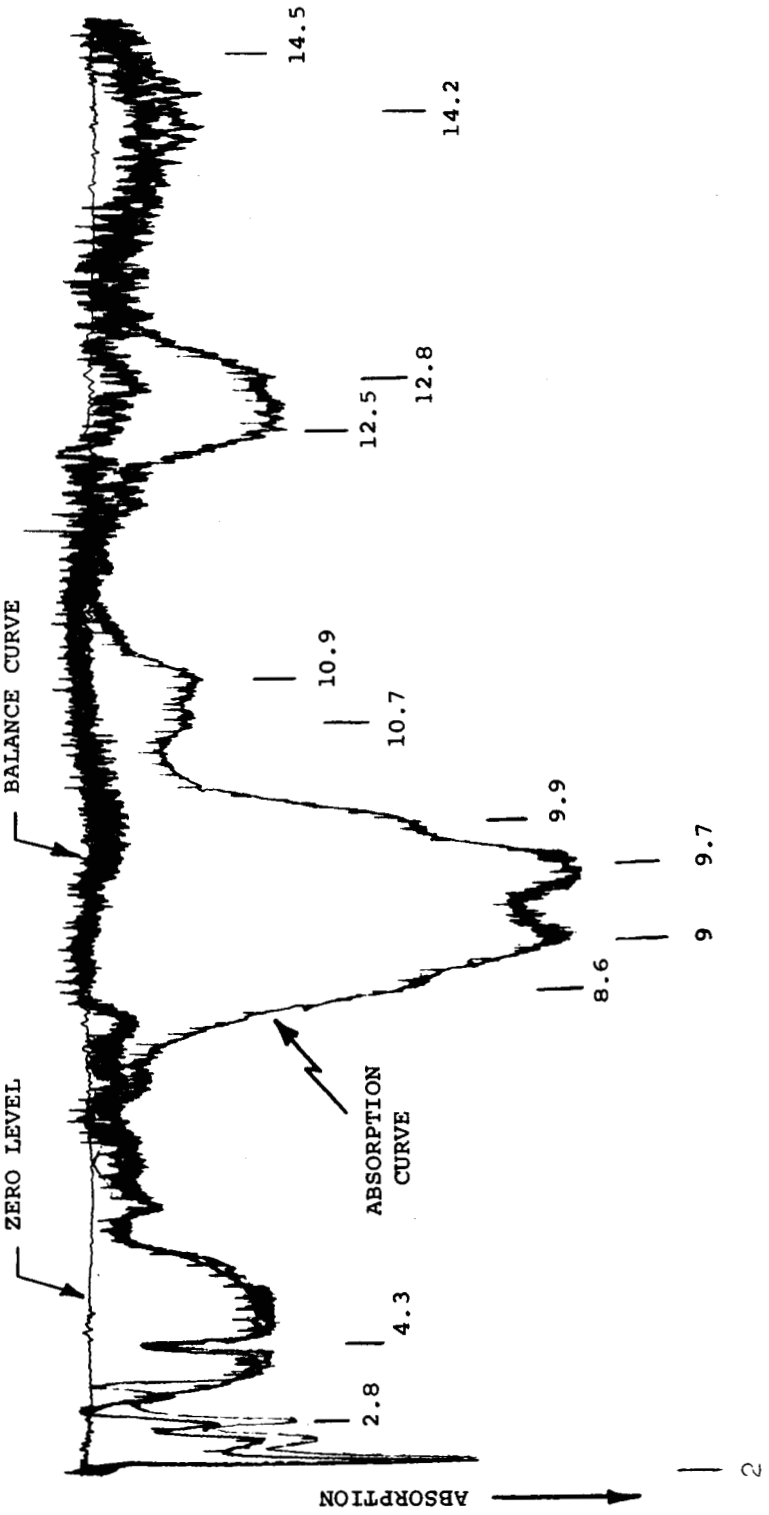

Figure 14: Absorption Spectrum of Lo-Micron Silica Powder (10 - 20 μ diam.)

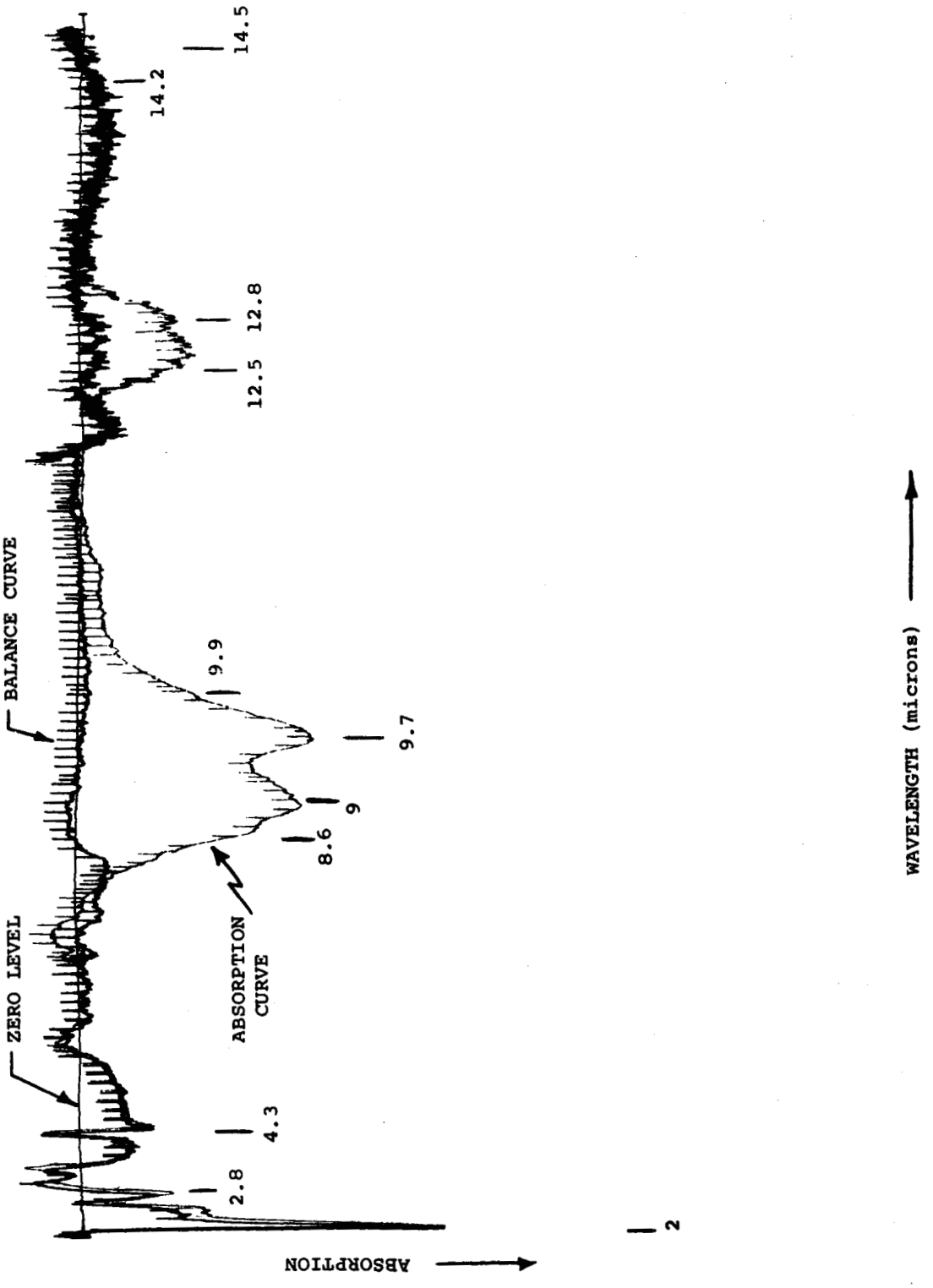

Figure 15: Absorption Spectrum of Lo-Micron Silica Powder (30 - 43 μ diam.)

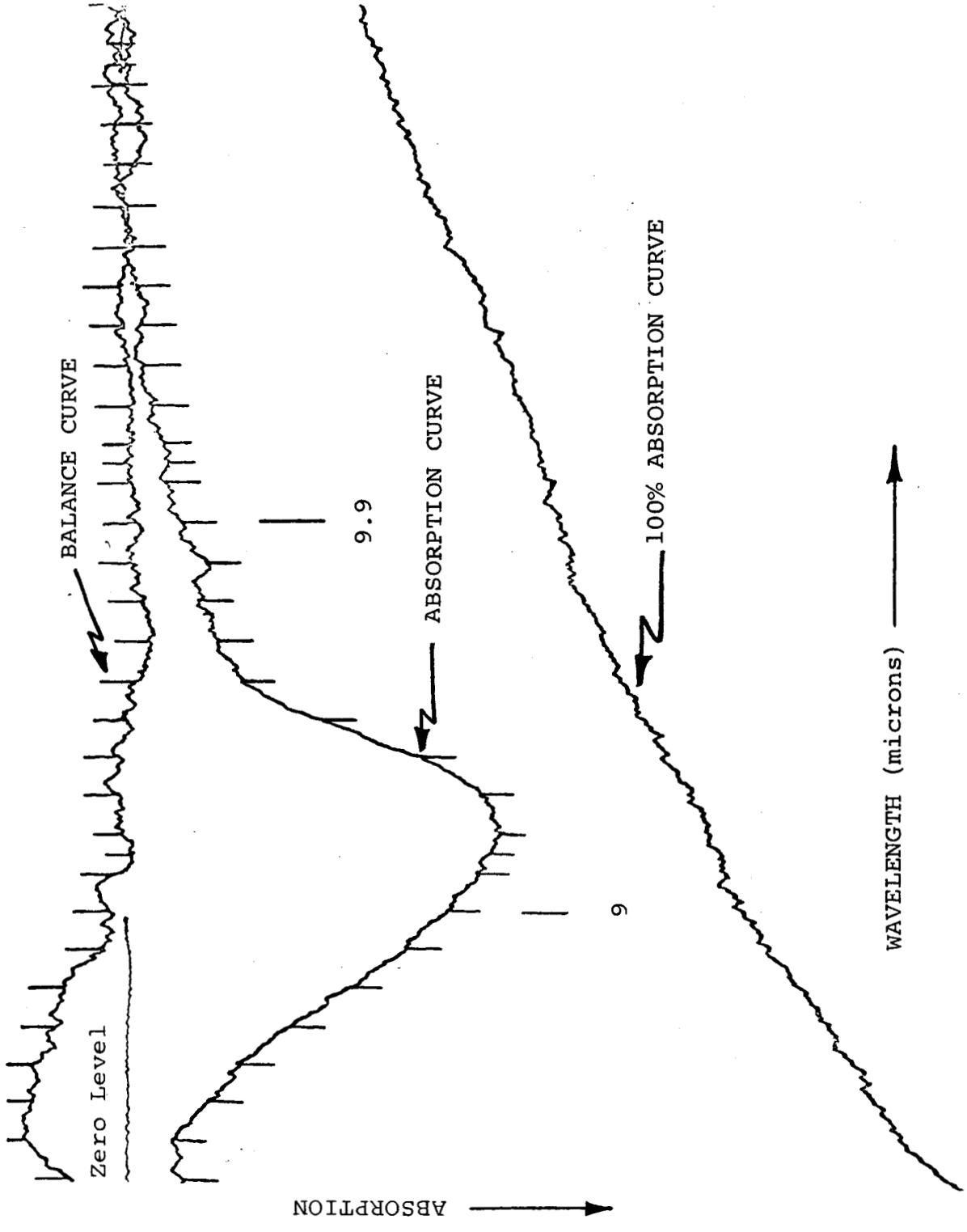

Figure 16: Absorption Spectrum of Quartz Powder, 0-150μ diam. (100 mesh)

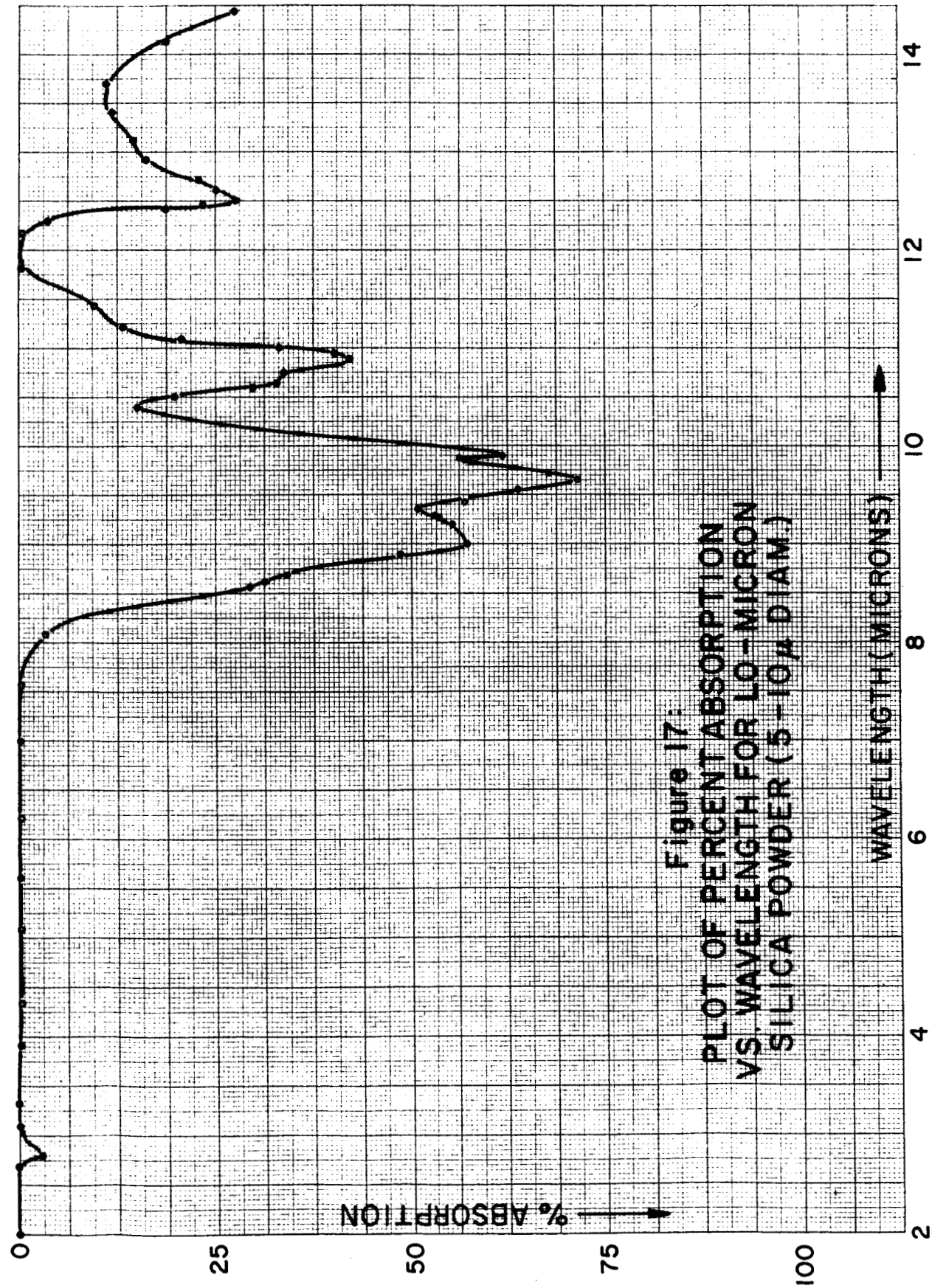

Figure 17: PLOT OF PERCENT ABSORPTION VS WAVELENGTH FOR LO-MICRON SILICA POWDER (5-10μ DIAM.)

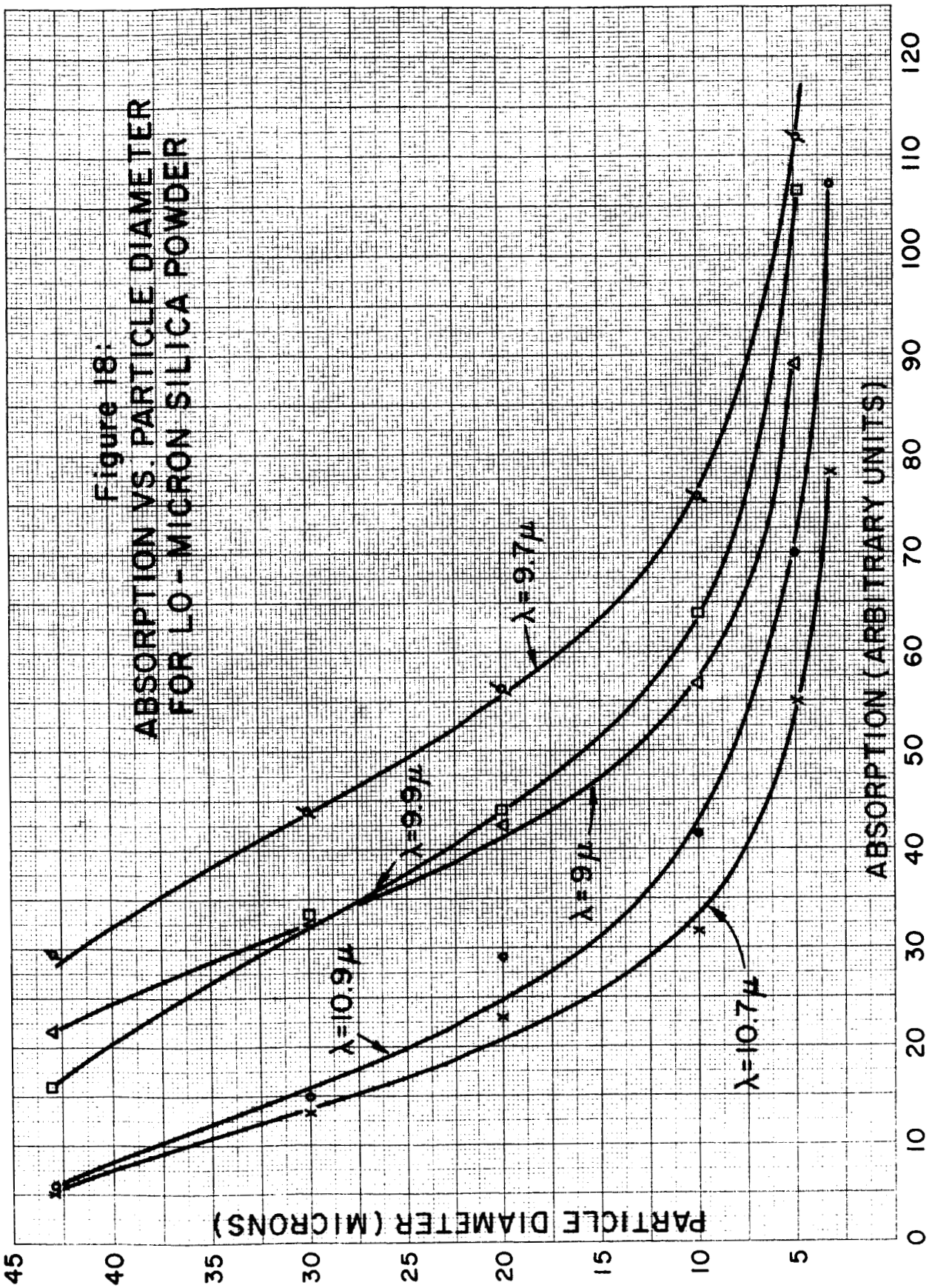
Figure 18:
ABSORPTION VS. PARTICLE DIAMETER
FOR LO-MICRON SILICA POWDER
ABSORPTION (ARBITRARY UNITS)
PARTICLE DIAMETER (MICRONS)
λ=9.7μ
λ=9.9μ
λ=9μ
λ=10.9μ
λ=10.7μ
0
10
20
30
40
50
60
70
80
90
100
110
120
45
40
35
30
25
20
15
10
5

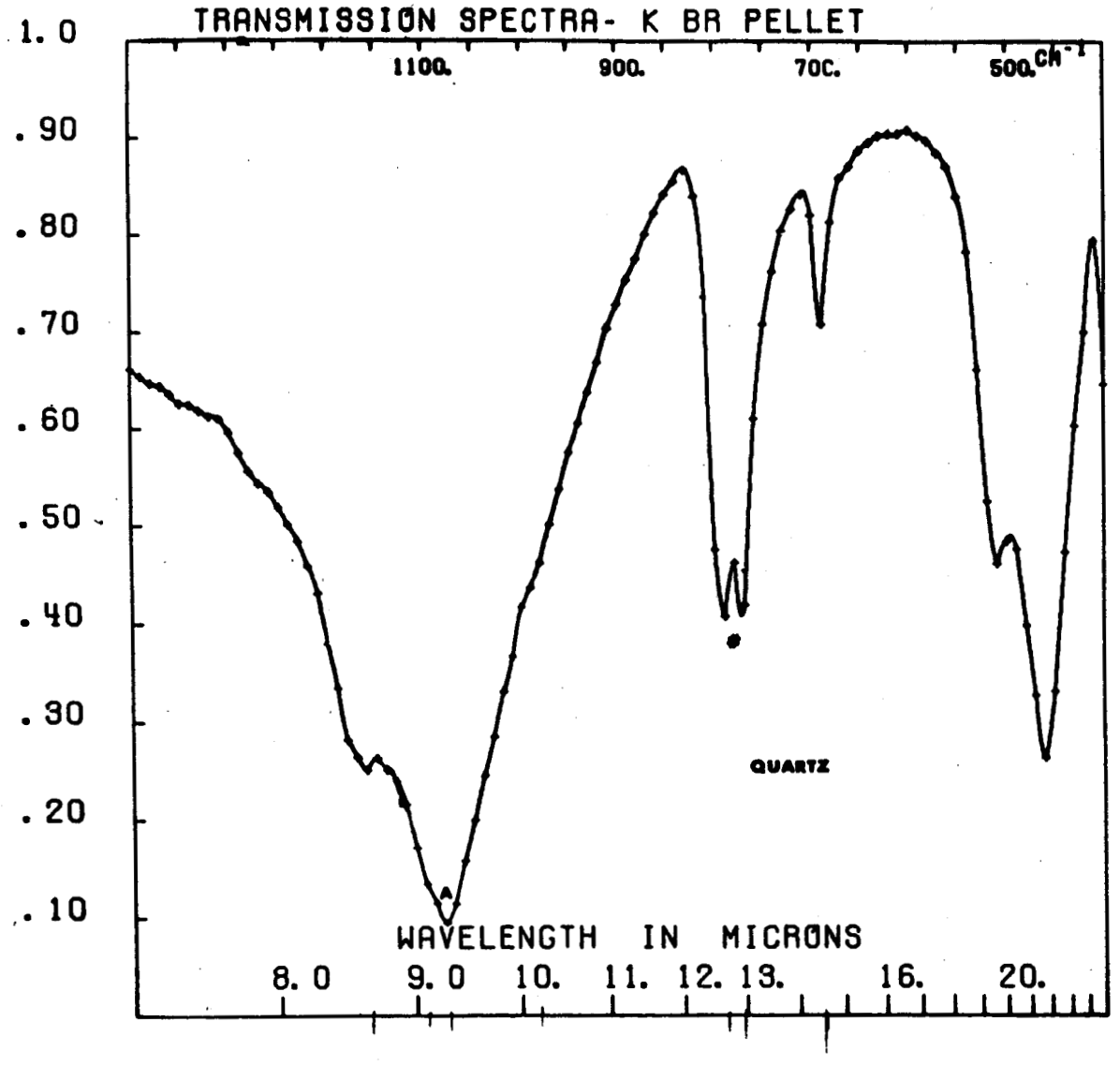

Figure 19: Transmission Spectrum of Finely Powdered Quartz in a KBr Pellet. (From Ref. 10)

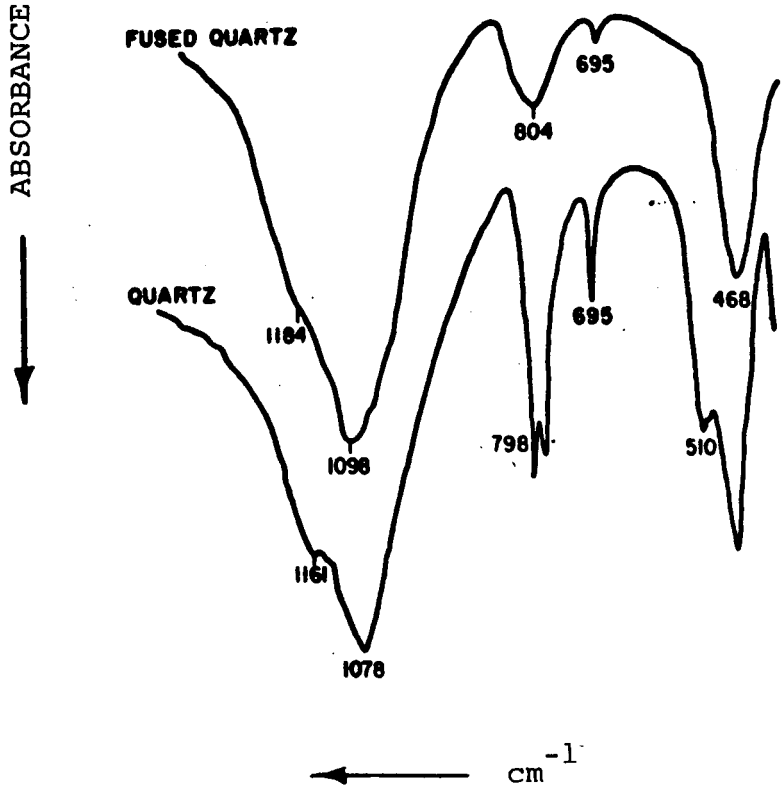

Figure 20: Absorption Spectra For Polymorphs Of SiO_2 - Quartz And Fused Silica. (From Ref. 10)

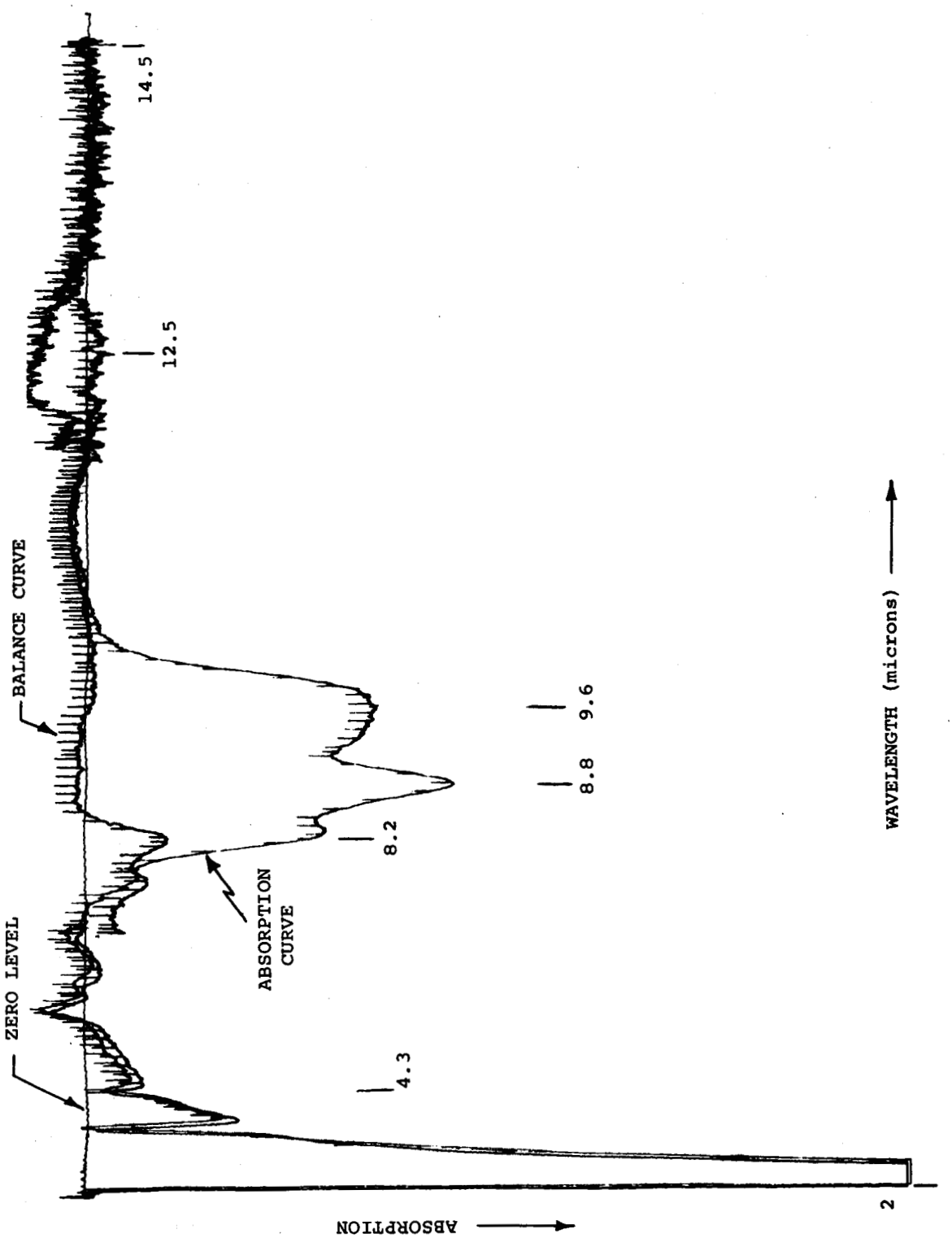

Figure 21: Absorption Spectrum of Frosted Fused Quartz Plate

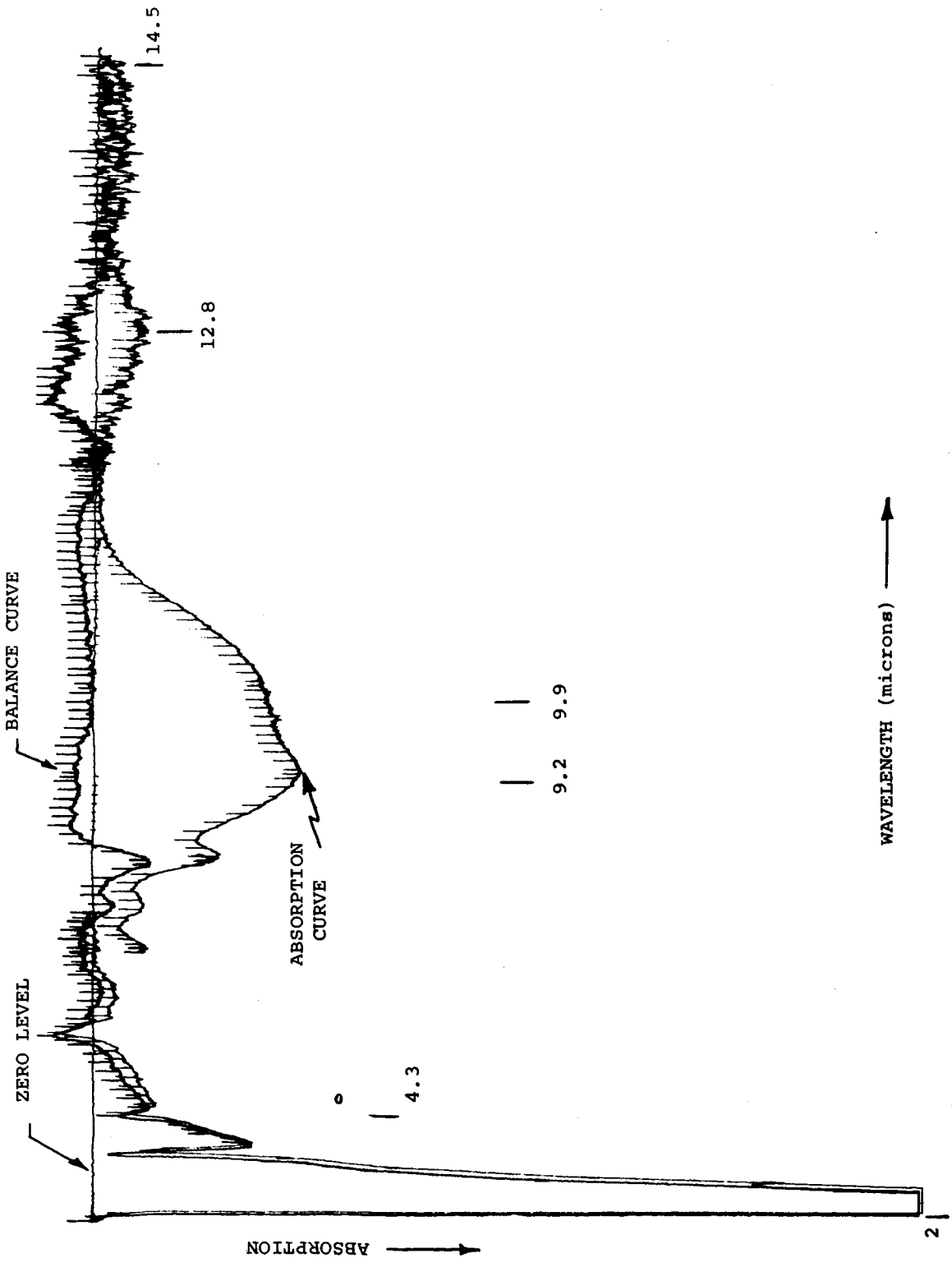

Figure 22: Absorption Spectrum of Frosted Soda Glass Plate

4. CONCLUSIONS

Task A. A balanced double-beam FMIR system (2 to 15 μ wavelength range), which included a Perkin-Elmer Model 12B monochromator, collimating optics and thermocouple detector, was fabricated. Spectra of the powder samples were obtained, and the characteristics of the absorption bands of each powder size were noted.

Of several cell material investigated, germanium was the cell material employed in this study; it is relatively durable and does not chemically react with the silica samples. The use of gallium arsenide cells would enable the useful optical wavelength range of the FMIR setup to be extended beyond 15 μ. Cells made of silicon can extend the range beyond 20 μ. The durability and hardness of these materials are comparable to those of germanium.

The germanium cells were cleaned by blowing the powder away with an air jet, brushing with a camel's hair brush, and washing with a mild detergent followed by swabbing with volatile solvents.

Extensive processing of the sample (e.g. mulling, optical polishing, making of pellets, etc.) was not required prior to analysis. All that was needed was close contact between sample and cell. Undue pressure of the rock samples on the specular surfaces could cause surface scratches which would result in light scattering, thereby decreasing the sampling power.

Task B. Lo-Micron Silica powder (0 to 43 μ in diameter) was

purchased from A. D. MacKay Inc. and separated into predetermined particle size groupings by means of air elutriation. Quartz powders, of diameters 0-300 μ (40 mesh) and 0-150 μ (100 mesh), were also obtained.

Task C. The FMIR absorption spectra of the powder samples were obtained and agree with those obtained by Lyon who used conventional absorption spectroscopy techniques.

Task D. No loss of power due to scattering was observed in the non-absorbing regions of the spectra. Had scattering occurred, the absorption curve of the sample would not have reached the balance line on both sides of the molecular resonance absorption band; that is, scattering would have shown up as a wavelength dependent power loss. The obtained spectra show the sample absorption line returning to or near the balance curve in the non-absorbing regions. Since there was no evidence of scattering, no power loss dependence on particle size was measured.

Task E. The spectra of particles in the 10 to 50 μ diameter range are in close agreement with Lyon's data (Ref. 10) as to the number of absorption peaks present and the wavelength at which they occur. The total absorption of each particle size decreased with increasing particle diameter. This may be due to an effective decrease in the volume of powder being sampled by the penetrating radiation, as the particle diameter increases. Since there are more voids between particles as diameter increases, the packing fraction decreases. All spectra exhibited high spectral contrast.

High contrast spectra of powdered quartz, of diameters 0-300 μ (40 mesh) and 0-150 μ (100 mesh), were obtained.

Task F. Samples of soda glass plate and fused quartz plate, frosted by grinding with a 240 mesh alumina/H_2O mixture, were examined by the FMIR technique. The obtained spectra were of high spectral quality.

Based on these experimental results, it is concluded that the technique of FMIR spectroscopy is a feasible method for obtaining high quality infrared absorption spectra of powders.

5. RECOMMENDATIONS

The results obtained with the powdered silicates are encouraging and strongly indicate that internal reflection spectroscopy can be of value in lunar soil analysis as well as in other areas not amenable to conventional spectroscopy techniques. It is recommended that these studies be continued, so that a thorough understanding of the interaction of the penetrating electromagnetic field with the powder samples may be obtained. The following is proposed:

a. Modify the balanced double-beam setup so that the angle of incidence can be continuously adjusted, and mount the cells in a vertical position so that they can be dipped into the powder.

b. Repeat measurements of powder samples using polarized light at various angles of incidence.

c. Attempt to obtain theoretical understanding of light scattering (or lack of it) for total internal reflection.

d. Extend measurements to wavelengths beyond 14.5 μ.

These measurements should provide valuable empirical knowledge of the effects of light scattering as related to internal reflection spectroscopy and perhaps encourage further investigation of scattering theory for total internal reflection.

It is suggested that the proposed work be considered a follow-on effort.

6. REFERENCES

1. Harrick, N. J., "Phys. Rev. Letters", 4, 224, 1960; "J. Phys. Chem.", 64, 1110, 1960.

2. Fahrenfort, J., "Spectrochim. Acta", 17, 698, 1961.

3. Fahrenfort, J., Visser, W. M., "Spectrochim. Acta", 18, 1103, 1962.

4. Harrick, N. J., "Ann, N. Y. Acad. Sci.", 101, 928, 1963.

5. Harrick, N. J., "Analytical Chemistry", Vol. 36, p. 188, Jan. 1964.

6. Becker, G. E., Gobeli, G. W., "J. Chem. Phys", 38, 2942, 1963.

7. Sharpe, L. H., "Proc. Chem. Soc. (London)", 1961, 461.

8. Sullivan, M. W. et al., "J. Electrochem. Soc.", 110, 412, 1963.

9. Philips Laboratories, Division of North American Philips Company, Inc., "Final Report For Research on Detection of Trace Quantities of Toxic Materials", Briarcliff Manor, N. Y., Aug. 1964.

10. Lyon, R. J. R., "Final Report on the Evaluation of Infrared Spectrophotometry for Compositional Analysis of Lunar and Planetary Soils" p. 73 Part I, p. 83 Part II, Stanford Research Institute, Sept. 1962 (I), Feb. 1964 (II).